Estuarine, Coastal and Shelf Science
May 2023, Volume 285 Pages 108309 (17p.)
https://doi.org/10.1016/j.ecss.2023.108309
https://archimer.ifremer.fr/doc/00833/94501/

Numerical modelling of tidal sediment dynamics in the Bay of Brest over the Holocene: How the use of a process-based model over paleoenvironmental reconstitutions can help understand long-term tidal deposits?

Olivier Matthieu [1, 2, 3, *], Leroux Estelle [4], Granjeon Didier [3], Le Hir Pierre [2], Rabineau Marina [4], Le Roy Pascal [6], Simplet Laure [5], Ehrhold Axel [1], Muller Héloïse [2]

[1] IFREMER/IUEM – ASTRE Laboratory – UMR Geo-Ocean, Pointe Du Diable, 29280, Plouzané, France
[2] IFREMER – DYNECO/DHYSED Laboratory, Pointe Du Diable, 29280, Plouzané, France
[3] IFP Énergies Nouvelles, 1 et 4, Avenue de Bois-Préau, 92500, Rueil-Malmaison, France
[4] IFREMER/IUEM – GIPS Laboratory – UMR Geo-Ocean, Pointe Du Diable, 29280, Plouzané, France
[5] IFREMER/IUEM – ODYSC Laboratory – UMR Geo-Ocean, Pointe Du Diable, 29280, Plouzané, France
[6] IFREMER/IUEM – ASTRE Laboratory – UMR Geo-Ocean, Pointe Du Diable, 29280, Plouzané, France

* Corresponding author : Matthieu Olivier, email addresses : molivier7777@gmail.com ; molivier@ifremer.fr

Abstract :

Long-term sedimentary infill of tide-dominated estuaries remains poorly understood. The main issue is the time-scale gap between the tidal process (hourly variations) and sedimentary layer formation (hundreds to thousands of years). Hydrodynamics induced by tides are responsible for intense remobilization of sedimentary layers inside estuaries and thus only partial sedimentary records are available. This consequently complicates understanding and interpreting the influence of hydrodynamic forcings via the preserved sedimentary deposits, as well as their chronology. Numerical modelling would appear to be the most-appropriate solution to overcome the lack of sediment deposit preservation. Hydro-sediment modelling explicitly simulates the impact of tidal processes on sediments. However, simulations time-span of these models are currently limited to decades, without simplification or schematization of the tide impact on sediments. This study (and Olivier et al., 2021) exposes a methodology exploring the evolution of sediment dynamics induced by tide over large time-scales (e.g. a transgression, ~10 ka). The aim is to use sedimentary records to identify and rebuild each key paleoenvironments of the sediment infilling in a tide-dominated estuary (defined as seafloor morphology and sea-level), in order to run them through hydro-sedimentary simulations (MARS3D/MUSTANG). The Bay of Brest is the area selected to test the methodology. Four paleoenvironments defined by distinct sea-level and seafloor scenarios are used to study the evolution of tidal-current impact on the erosion/deposition patterns over the last 9000 years. Simulation results were compared with sedimentary records in terms of: sedimentation rates, distribution of erosion/deposition patterns (as deduced from seismic records) and distribution of grain-size classes (comparison with cores). Simulation results allowed to: (I) explain most of the sediment distribution for each sedimentary unit, reconstruct tide influence on the Holocene infilling of the Bay of Brest over 9 ka; (II) discuss the evolution of the influence of sediment supply sources; (III) highlight the spatial evolution of erosion and deposition, and the limit between cohesive and non-cohesive deposits, which evolve with tidal prism increase in relation to the active-flow section width in the Bay of Brest: when fast and significant expansion of the active-flow section width occurs (e.g. inundation of extended terraces becoming subtidal) those boundaries move down-estuary, while the opposite occurs when the increase of active-flow section width remains low during sea-level rise.

Highlights

► Set up of a methodology to explore the impact of tides on sedimentation over 9 ka. ► Tide-induced sedimentation is reconstructed over the Holocene in the Bay of Brest. ► Most of the sediment deposits in the Bay of Brest are supplied by oceanic borders. ► Sandy/muddy deposition limit varies with the tidal prism/active flow section ratio.

1. Introduction

Tides are a key process in the understanding of sediment dynamic in many coastal areas throughout the world, particularly in bays and estuaries. Although they cover a relatively small percentage of all sedimentary environments, bays and estuaries are located at the interface between rivers and continental shelves. They are consequently a key area in the transfer of sediment from source to sink. How and how much do estuaries trap sediments over long time intervals (few centuries to tens of thousands of years) is therefore an important question to answer in order to understand estuaries and ocean basin stratigraphy. Yet tide-dominated estuary infill remains poorly understood because sedimentary records are often only partially preserved. Processes acting on sediment transport in tide-dominated estuaries are very complex, as they are influenced by numerous hydrodynamic and sedimentological factors over a wide range of temporal and spatial scales (Wang, 2012). Tidal sedimentary rocks are the result of hundreds to thousands of years of a short temporal scale forcing, as tidal currents vary on an hourly scale. Water flow patterns evolve with sea-level variation and sediments are thus reworked repeatedly during the long-term infilling of an estuary. It is therefore very complicated to discretize the different events and understand the evolution of the system (Tessier et al., 2012). The stratigraphic response of estuaries to sea-level variation is even more complicated to understand, as it varies according to the combination of sea-level variation rates, sediment supply, bedrock morphology, and hydrodynamics (Tessier, 2012). The stratigraphic interpretation of tidal deposits is carried out by analogy with present-day observations (*e.g.* Reynaud et al., 2006; Shanmugam et al., 2009; Flemming, 2012; Olariu et al., 2012; Reynaud and James, 2012; Lee et al., 2022), which are summarized in conceptual models (*e.g.* Dalrymple and Choi, 2007; Dalrymple et al., 2012). The interpreted depositional environments are assembled to determine the depth and influence of hydrodynamics by analogy. In estuary sequence stratigraphy, transgressive and regressive movements are linked to the interpreted evolution of shoreline, which comes from depositional environment interpretation of the sedimentary record (*e.g.* the intertidal mud/sand limit, sand bars, salt marsh). Due to poor preservation, it is unusual to observe longitudinal variation of facies deposits, even in the presence of a large dataset (*e.g.* cores, seismic, outcrops, Tessier, 2012). The combination of diachronous facies boundaries (Dalrymple and Zaitlin, 1994), poor preservation of deposits, the great variability of facies and hydro-sediment processes in estuaries, substantially complicates establishing common patterns for different stages of sea-level rise. This was demonstrated in a synthesis of tide-dominated estuary Holocene infill, made by Tessier (2012). The hydro-sediment response of estuaries to long-term parameters (over hundreds to thousands of years), such as sea-level or seafloor evolution between sedimentary units, is often hard to explain with only preserved sediment records.

Physical scale models have been used for many years (*e.g.* Price and Kendrick, 1963) for simulating morphological changes at engineering time scales (a few days to decades), but cannot be used to simulate geological time scales (1 to 10 ka) while still respecting the very short time scale of tidal forcing. On the other hand, process-based numerical modelling can be considered to study the effect of tides on sediment dynamics in estuaries. However, the time step imposed by hydrodynamic processes acting in estuaries generally prevents the simulation of long periods (usually simulations from hours to decades, *e.g.* Bárcena et al., 2016; Grasso and Le Hir, 2019; Tosic et al., 2019). The temporal scale limit of hydro-sediment modelling is an important scientific lock, because transgressions last about ten thousand years and the formation of sedimentary units around hundreds to thousands of years (Dalrymple et al., 1992; Tessier et al., 2012). To overcome this time scale issue, many techniques have been developed to simulate longer time intervals (around thousand years maximum). A synthesis of these techniques is proposed by Roelvink (2006). The most used technique is to apply a multiplicative factor (n) for erosion and deposition fluxes, or the net erosion/deposition, estimated by a hydro-sediment model (*e.g.* Franz et al., 2017; Le Tu et al., 2019; Elmilady et al., 2020). Some studies have used a very high morphological factor to approach time intervals in the order of a thousand years. Mainly conceptual estuaries were simulated over such long periods and they all led to estuary equilibrium configuration (Lanzoni and Seminara, 2002; Bolla Pittaluga et al., 2015; Guo et al., 2015; Braat et al., 2017). Simulations of Bolla Pittaluga et al. (2015) indicated that the investigated system always moves toward an equilibrium configuration in which the net sediment flux in a tidal cycle remains constant throughout the estuary and equal to the constant sediment flux delivered by the river. Regardless of the definition of dynamic equilibrium (see Zhou et al., 2017), most of sediment features, such as tidal channels, dunes and tidal flats, are the result of a system seeking to reach its dynamic equilibrium (Coco et al., 2013). With eustatism or subsidence processes keep changing the conditions expected to reach a dynamic equilibrium. In order to study the formation of sediment layer at geological time scale the main objective is then to understand the hydro-sediment response to new conditions. Moreover, according to Zhou et al. (2017), an equilibrium configuration can be reached only in the "virtual world: where systems of equations are solved and the solution of the system is in fact the equilibrium configuration", and not in the "real world, where variability in the environmental drivers and landscape settings often precludes the system from reaching an equilibrium condition".

To overcome equilibrium problems between simulations and “real word”, studies from Imperial college have already analyzed past tide influences on sediments at large spatial (sedimentary basin to global) and temporal scales (about 10-50 Ma, *e.g.* Wells et al., 2007a; Mitchell et al., 2010; Wells et al., 2010). By using the hydrodynamical ICOM model (Imperial College Ocean Modelling) for short time intervals (days to months), hydrodynamic simulations were linked to sedimentary records with bed shear stress calculation over paleoenvironmental reconstructions (*e.g.* Cretaceous, Bohemian basin, Mitchell et al., 2010; late Oligocene-Miocene, South China Sea, Collins et al., 2018; late Pennsylvanian Seaway of NW Eurasia, Wells et al., 2007a; 2007b). Other studies have explored recent and old paleoenvironmental impact on tidal propagation, such as Reynaud and Dalrymple (2012, Holocene and Lower Cretaceous, and Zuchuat et al., 2022, lower Oxfordian).

Our study exposes an innovative methodology to explore the influence of paleoenvironmental evolution (seafloor and sea level) on the sediment dynamics of tide-dominated estuaries. We propose to use hydro-sediment modelling at several stages of a marine transgression. The innovative aspect of our study is that the reconstructed scenarios (relying on sediment records) represent all the key stages of estuary infilling and therefore allow to discuss the evolution of the hydro-sediment dynamics between the scenarios and their triggers. The objective of this study is to observe the hydro-sediment response of an estuary to geological parameters, such as seafloor morphology and sea-level evolution, and identify main triggering factors of hydro-sediment dynamics evolution. Our methodology is applied to the evolution of the Bay of Brest over the Holocene, from 9 ka BP to present-day. This work follows a previous paper (Olivier et al., 2021) dedicated to changes in tidal hydrodynamics linked to morphological and mean sea-level evolutions.

The methodology, described in section 2, is based on the use of a numerical hydro-sediment model (MARS3D-MUSTANG), over paleoenvironmental scenarios. Section 3 presents simulation results for each scenario and a reconstruction of the impact of tides on the Bay of Brest infilling during the Holocene. The following discussion (section 4) focuses on two points: (i) the influence of sediment supply sources and (ii) the impact of environmental conditions (seafloor and sea-level) on sediment deposits or erosion induced by tide. Conclusion are set in section 5.

2 Methodology and tools

2.1 The modelling strategy

This paper aims to explore the long-term evolution (a transgression, *i.e.* about 10 000 years) of a tide-dominated estuary in response to sea-level rise and seafloor evolution. With only partial sedimentary records and no hydrodynamic data in the past, the idea is to use numerical modelling to reconstruct tidal currents, sediment flows and erosion/deposition trends, which can be compared to available sediment records. In order to study the evolution of hydro-sediment dynamics at geological time scale, successive scenarios are built. Each scenario is representative of large time intervals (centuries to a few thousands of years) and is generated for each major change of paleoenvironments, or sediment dynamics. A scenarios is characterized by a specific seafloor map (rebuilt by backstripping using thickness maps derived from seismic data) and a mean sea-level (Goslin et al., 2015; García-Artola et al., 2018). Hydro-sediment modelling is run on each scenario to simulate tidal currents and to locate the erosion and deposition areas for grain-size class. Simulation results are compared to sedimentary records to calibrate sediment supply and validate global trends: the simulated evolution of sediment fluxes, erosion and deposition areas are compared to thickness maps of sedimentary units, and surficial sediments distribution are compared to cores data. Once calibrated, the succession of these representative geological scenarios provides information on deposit preservation from one scenario to the other, spatial evolution of grain-size classes and triggers of main hydro-sediment dynamic changes. This methodology allows to upscale hydro-sediment dynamics over long time interval, and study the evolution of tidal deposits and paleoenvironments during an estuary flooding and infilling.

2.2 The Bay of Brest

The Bay of Brest is a semi-enclosed macrotidal bay located at the western end of Brittany, France (Fig. 1). The mean spring tidal range is 5.9 m and the mean neap tidal range is 2.8 m in Brest harbour (Beudin, 2014). The Bay is protected from ocean waves by the strait between Plouzané and the Roscanvel peninsula (1.8 km wide, connecting the Bay and the continental shelf). This configuration induces a very weak swell climate compared to the wave energy regime outside the Bay (Iroise Sea, Monbet and Bassoullet, 1989; Olivier et al., 2021). The study area also displays a short fetch (~25 km, Stéphan et al., 2012), protecting it from significant wind-induced waves.

During the Tertiary era, glacio-eustatic movements generated transgressions and regressions around the Brittany region. The Bay of Brest emerged several times during low sea-level stages and the basement is eroded by paleo-rivers since the Oligocene (Hallegouet et al., 1994). Past fluvial systems generated three morphological domains (Gregoire et al., 2016, Fig. 1): T1 is the main paleo channel; T2 is the first stage of terraces, above T1; T3 corresponds to the shallowest terraces localized in sheltered coves and bays. A network of secondary channels within T2 and T3 connects these domains to the main channel T1 (Fig. 1). The surrounding land of the Bay of Brest are mostly made of hardly erodible magmatic and metamorphic rocks, and has suffered only minor weathering and erosion over the last 9 ka. The limit between the Bay sensu stricto and the surrounding land could be considered as a fixed land boundary. The accommodation space in the Bay of Brest is thus mainly controlled by the shape and location of T2 and T3.

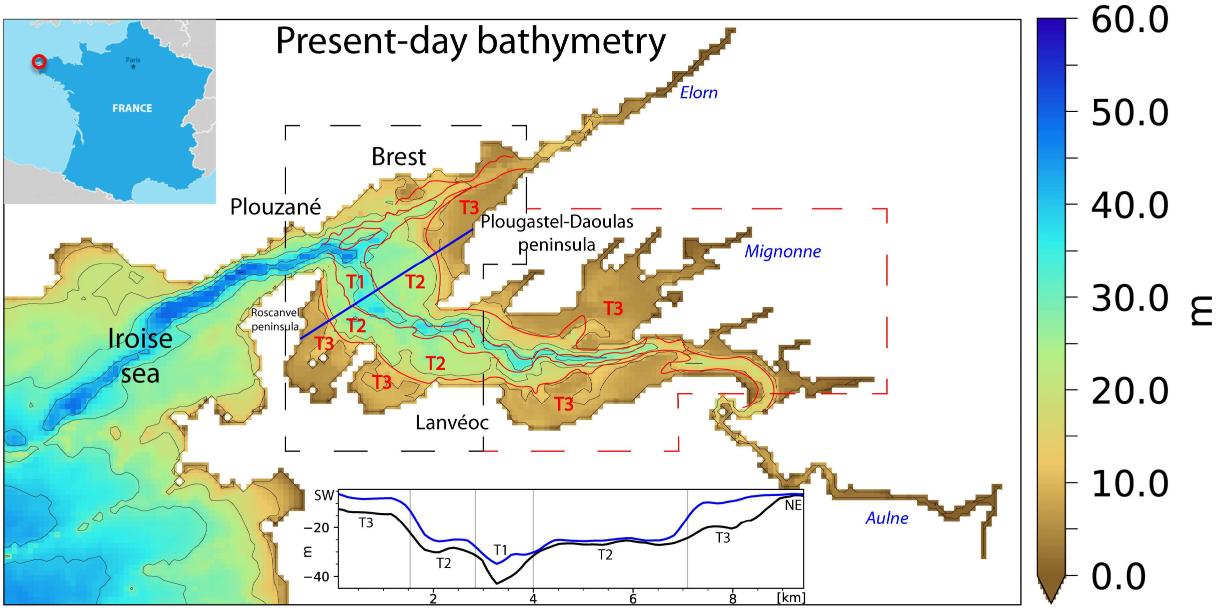

Fig. 1 : Present-day bathymetric map of the Bay of Brest, generated from SHOM data (2015). The inset-bathymetric section is indicated by a blue line on the map. On this section, the blue line corresponds to present-day bathymetry and the black line to the beginning of the Holocene infilling of the Bay of Brest (9 ka BP). T1: paleo main channel. T2: deepest stage of terraces. T3: shallowest stage of terraces (delimited by red lines). Black dotted box represents the limits of the central area and red dotted box shows the limits of the upper area of the Bay.

This estuary is well suited to explore tidal impact on hydro-sediment dynamics, because of its specific characteristics: I) it is a macrotidal system, II) it is protected from ocean waves and III) it has a specific seafloor morphology (three different morphological domains), providing observation of the influence of several paleoenvironmental configurations. In this study, the estuary is divided into two parts: the upper part, to the east of the strait between Lanvéoc and the Plougastel-Daoulas peninsula (towards the estuary of the Aulne river, Fig. 1), the central part is delimited by the same strait to the east and the one between Plouzané and Roscanvel peninsula to the west. This strait behaves like a bottleneck in terms of hydro-sediment processes. All areas westward of this strait (Plouzané-Roscanvel) such as the Iroise Sea, are affected by waves and storms and therefore are not analysed in this paper (Fig. 1). The three most important rivers are the Aulne, the Elorn and the Mignonne.

Over the Holocene, the evolution of river sediment supply is unknown and only proxies can give clues on regional climate evolution. The Early Holocene (11.7 to 8.2 ka BP) is characterized by high summer insolation values and is still strongly impacted by the remanent presence of continental ice-sheet that developed during the last ice age (Lambert, 2017). The vegetation then gradually grew around the Bay of Brest (Lambert, 2017) and precipitations increased in northern Europe (Seppä and Birks, 2001; Bjune et al., 2005), in connection with a climate warming during the Holocene climate optimum between 8.2 to 4.2 ka BP (Koshkarova and Koshkarov, 2004). Penaud et al. (2020) suggest that the stronger humidity is linked to the North Atlantic Current, which may have amplified seasonal continental humidity in western France during the Holocene climatic optimum. After this climatic optimum, temperatures globally decreased (Berger and Loutre, 1991) and precipitations slightly decreased in northern Europe (Seppä and Birks, 2001; Bjune et al., 2005). This time interval also saw an important expansion of agriculture in the region inducing deforestation and therefore a greater runoff from the land towards rivers (Lambert, 2017). Those studies highlight an important evolution of river sediment supply in the bay of Brest, while oceanic supply is totally unknow even at the present-day.

2.3 Modelling scenarios

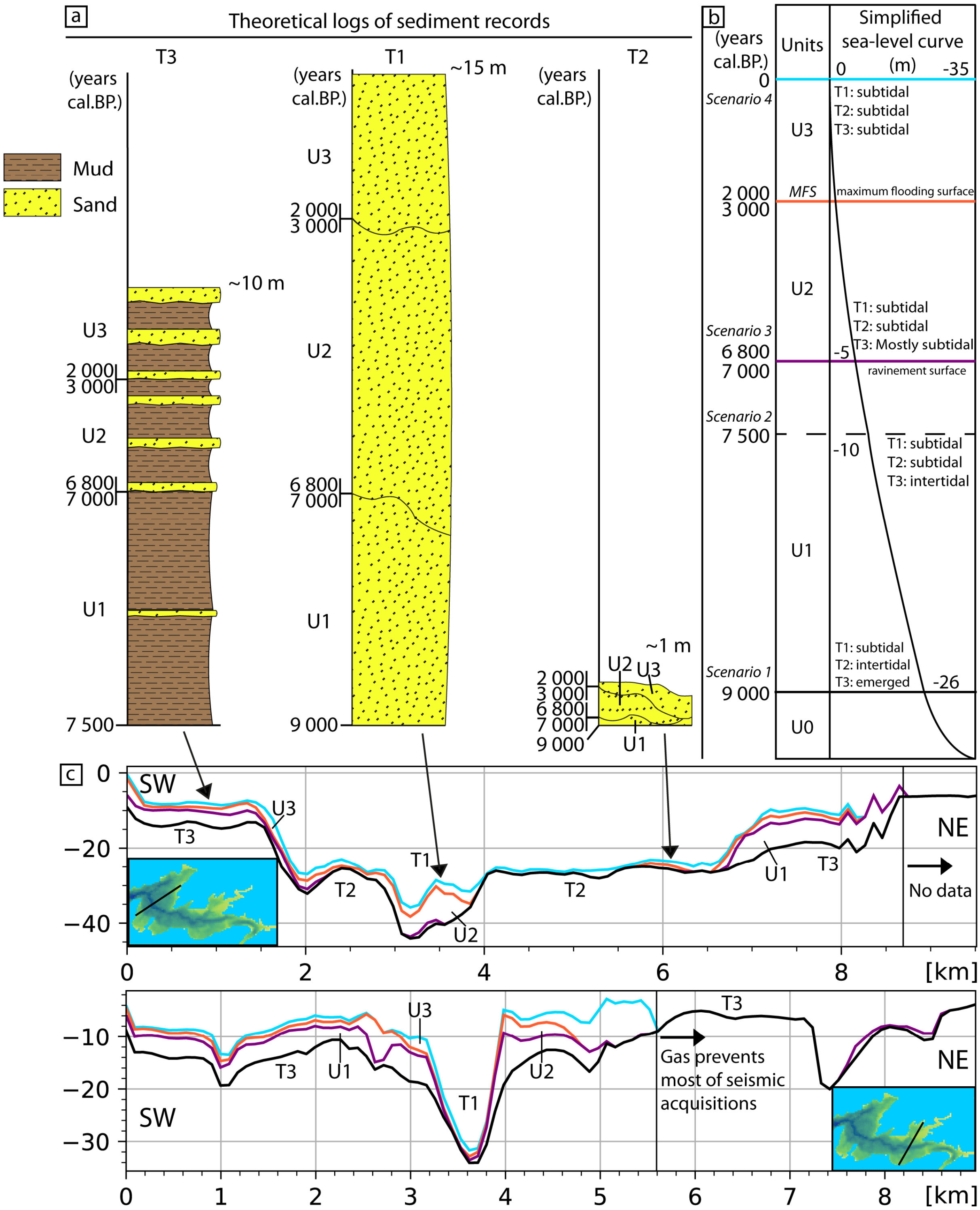

Fig. 2: a: theorical logs for each morphological domain over the Holocene time interval in the Bay of Brest (from the interpretation of 10 cores and previous study of Gregoire, 2016). Muds are displayed in brown and sands in yellow. b:

Sedimentary units chronology (from Grégoire, 2016) and simplified sea-level curve over the Holocene. c: two sections present the depth of each sedimentary unit top, relative to the present-day mean sea level: black line for the top of U0, purple for the top of U1, orange for the top of U2 and light blue for the top of U3 (top corresponding to well-defined and main stratigraphic surfaces, see Gregoire et al., 2017). Correspondence between sea-level positions and sediment elevations is provided for each scenario in Fig. 13.

The Holocene infilling of the bay of Brest can be described by four sedimentary units (Gregoire, 2016; Gregoire et al., 2017): U0 (~10-9 ka cal. BP, LST), U1 (~9-7 ka cal. BP, TST), U2 (~6.8-3 ka cal. BP, TST) and U3 (~2-0 ka cal. BP, HST, Fig. 2). U0 is a fluvial dominated unit characterized mainly by fluvial incision and deposition. We therefore focused our study on the tidal infilling of the bay of Brest, from 9 ka BP to present-day, that is during U1, U2 and U3. Four scenarios are defined to represent these three units and the main stages of sediment infilling over the Holocene transgression in the Bay of Brest (Olivier et al., 2021). Each scenario is defined by a major change in stratigraphic patterns (deposit dynamics) and after each important retreat of the coastline, such as the flooding of a new morphological domain.

U1 is characterised by a wide range of sea-level variations during its deposition from -26 to -5 m (Fig. 2) and therefore two scenarios are generated for this sedimentary unit. Scenario 1 is set at the beginning of this time interval at 9 ka BP, with a seafloor corresponding to the top of U0. During this scenario the intertidal area is located over T2 terraces. Scenario 2 is set at 7.5 ka BP and aims to represent the end of U1. The chronology inside sedimentary units is poorly known and thus the selected seafloor for scenario 2 is the top of U1, as the aim is to explore hydro-sediment dynamics conditions at the beginning of U1 with scenario 1 (9 - 7.5 ka BP) and the end of U1 with scenario 2 (7.5 - 7 ka BP). The intertidal area is over T3 during scenario 2. Then, during U2 deposition the rise in sea-level slows down (-5 to 0 m). The configuration (seafloor and sea-level) remains similar during this time interval (6.8 - 3 ka BP) and thus scenario 3 aims to represent the entire deposition time interval of U2. Scenario 3 is set at 6.8 ka BP, with the top of U1 as the seafloor. During scenario 3 almost all T3 terraces are subtidal. During U3, sea-level remains close to that of the present-day (Fig. 2) and thus only one paleoenvironment is generated to represent U3. Scenario 4 is set at the present-day and aims to represent the entire deposition time interval of U3 (2 - 0 ka BP), which is still active at the present-day. Present-day seafloor (top of U3) and sea-level are used for this scenario. During the Holocene, preserved mud deposits are mainly localised over T3 and most of the preserved sand deposits are localised over T1 (Fig. 2). These four scenarios represent a different paleoenvironmental configuration and are thus defined by a seafloor morphology, and a mean sea level. All details on sediment data and bathymetric maps generation (Tab. 1) used for the construction of these four scenarios, are provided in Olivier et al. (2021).

Tab. 1: Summary of scenario settings

Scenario (simulation aim)	Scenario 1 (Beginning of U1)	Scenario 2 (End of U1)	Scenario 3 (U2)	Scenario 4 (U3)
Age	9 000 years BP	7 500 years BP	6 800 years BP	Present-day
Mean sea-level (compared to present-day)	-26 m	-10 m	-5 m	0 m
Seafloor	Top U0	Top U1	Top U1	Top U3 (present-day seafloor)

2.4. The hydro-morpho-sediment model MARS3D-MUSTANG

The sediment module, MUSTANG, is coupled with the hydrodynamic model MARS3D (Lazure and Dumas, 2008). The hydrodynamic code MARS3D computes the hydrodynamic variables (currents, free-surface elevation) and MUSTANG computes sediment transport, erosion and deposition processes and morphological evolutions in coastal and estuarine environments (Le Hir et al., 2011; Mengual et al., 2017). The hydrodynamic settings are available in Olivier et al. (2021). For each of the four scenarios, simulations are forced by tides and river water discharges only, without accounting for waves due to the sheltered position for oceanic waves and the short fetch of the Bay. The present-day tidal forcing extracted from the SHOM CST-France (Le Roy, R., Simon, B., 2003) is used for each stage. That choice is justified by similar tidal amplitudes along Brittany coast (Goslin et al., 2015) and the European continental shelf (Uehara et al., 2006; Ward et al., 2016) during the period 10 ka BP to present-day (see Olivier et al., 2021).

The horizontal computation grid is cartesian, with a mesh-size of 250 m x 250 m and the water column is composed of 20 levels. This very fine vertical resolution results from previous applications of MARS3D in the Bay of Brest (Klouch et al., 2016; Frère et al., 2017; Petton et al., 2020). Given the time dedicated to the implementation of the grid and the validation of hydrodynamics, a similar configuration is used in this study. In the water column, the model resolves advection/diffusion equations for different classes of particle (in a 3-D framework for mud and in a 2D framework for sands). Although coarse non-cohesive sediments are transported as bedload, the ability of the model to simulate their dynamics by considering transport in suspension was previously demonstrated using a fitted erosion law (Le Hir et al., 2011; Dufois and Le Hir, 2015). The model accounts for the transport of four sediment classes: gravels 3 mm; sands 1.1 mm; fine sands 200 μm and muds 15 μm. The selection of these representative grain-size classes is based on previous work (Gregoire, 2016) and on the study of 10 sediment cores. For each class, grain density is 2600 kg/m^3 (quartz density).

The sediment model has the same horizontal resolution as the hydro-dynamic model and manages up to 100 sediment layers, with variable thicknesses between 1 μm and 1 cm (excluding the deepest layer, which can be thicker), according to deposition and erosion events. This discretisation of the sedimentary column enables to respect the vertical gradients of sediment composition, without excessive mixing that would occur in a thick layer (Le Hir et al., 2011). When the maximum number of layers is exceeded, the two deeper ones are merged. The initial sediment bed has a uniform thickness of 0.5 m inside the Bay (no erodible sediment outside the Bay), and is uniformly composed of 10% gravel, 20% sand, 30% fine sand and 40% mud (definition based on the cores described by Gregoire, 2016). The basement is located below this initial sediment layer and is not erodible. The basement is presumed to be coarse continental sediment at the beginning of sediment infilling in the Bay of Brest 9 000 years ago (Gregoire, 2016). The skin roughness is assumed to be uniform and constant for all simulations, and equal to 1 mm, corresponding to coarse sediment. The choice of a uniform roughness length avoids the generation of misleading flow patterns with a poorly validated parameterisation and facilitates the comparison between scenarios. The erosion flux (E) for sands and mud is expressed in a "Partheniades-Ariathurai" form (Nielsen, 1992):

$$\text{Eq. 1: } E_{sands} = E0_s \left(\frac{\tau}{\tau_{Ci}} - 1\right)^n$$

$$\text{Eq. 2: } E_{mud} = E0_m \left(\frac{\tau}{\tau_{Ci}} - 1\right)$$

with E0 the erodibility for mud ($E0_m$) or sands ($E0_s$), τ the bottom shear stress computed with the skin roughness, τ_{Ci} the critical shear stress for erosion (Tab. 2) and n a power coefficient applied to excess shear stress (= 1.5, according to van Rijn, 1994). A linear interpolation between sand and mud behaviour is used, depending on proportions of the mixture. Net sedimentation is driven by the excess of shear stress induced by the water flow on the seafloor, according to Krone's law:

$$\text{Eq. 3: } D_i = W_{si} C_i \left(1 - \frac{\tau}{\tau_{di}}\right)$$

where, for each sediment class i, D_i, sedimentation rate, W_{si} settling velocity, C_i near-bed suspended sediment concentration ($g.l^{-1}$) and τ_{di} critical shear stress for deposition ($N.m^{-2}$). Settling velocities of sans are computed from Soulsby (1997), while a constant average value of 0.5 $mm.s^{-1}$ is considered for mud, in order to schematically account for flocculation (Chataigner, 2018).

The value of τ_{di} is set very high for sands (1000 Pa) to allow full deposition, and chosen rather high (1 Pa) for mud to prevent its deposition when the bottom layer is very turbulent, as consolidation processes are not explicitly accounted for (Tab. 2). The primary consolidation of sediments is disabled for the sake of computing costs, and secondary consolidation is neglected, in agreement with the short duration of simulations, which is much shorter than the duration of diagenetic processes responsible for the long-term consolidation of sediment. Simulations are morphodynamic, which means that seafloor elevation is recomputed according to the erosion and deposition fluxes calculated. A previous numerical experiment with similar sediment layer model was conducted in the mouth of the Seine estuary, a macrotidal zone with the same size as the Bay of Brest: it was shown that after one year simulation starting from uniformly mixed sediment, a realistic distribution of sands and mud could be reconstituted in the surficial sediment (Lemoine and Le Hir, 2021). Initializing hydrodynamics takes a few days, but tidal currents need months to redistribute sediments which were initially uniformly distributed. One year of spin-up is required to initialize the surficial grain-size distribution, in agreement with the hydrodynamics of the period in a context where the nature of the bottom surface layer is uncertain. Based on this experience, our simulations of the Bay of Brest are carried out for a two-year period, but only the second year is analyzed.

Tab. 2: Hydro-sediment model parameter settings

Hydro-sediment model parameters	τ_{Ci} (Pa) (Olivier et al., 2021)			$E0_i$		τ_{di} (Pa) (Chataigner, 2018)	
Values	fine sand	sand	gravel	mud	sands	mud	sands
	0,147	0,541	2,072	0,003	0,01	1	1000

2.5 Sediment supply calibration on sedimentary unit volumes

To calibrate sediment supply, the only quantitative information available for the Bay is the volume of preserved deposits for each sedimentary unit, which is calculated from thickness maps. For each sedimentary unit, the positive balance between deposition and erosion for each grain-size class is recorded, *i.e.* when the quantity deposited is greater than the quantity eroded (preserved deposits). However, new hydrodynamic conditions can generate the erosion of previous sedimentary units a long time after their deposition. The amount of deposit eroded by subsequent hydro-sedimentary dynamics cannot be quantified and constitutes the greatest uncertainty in the study of past sediment systems. The calculated volume only accounts for the preserved part of sediment deposits, as the reworked fraction within sedimentary units is unknown.

For comparison with simulations over one year, the volumes of sedimentary units are converted into mean sedimentation rates over the Bay, depending on each sedimentary unit time span (Tab. 3). Sedimentation rates therefore rely on the sediment volume calculated from the thickness map of each unit, based on the seismic interpretation, and filling chronology of the Bay (Gregoire, 2016, Fig. 2).

Tab. 3: Preserved seismic unit volumes and annual sedimentation rate calculated.

Unit (ages)	U1 (9 to 7 ka BP)	U2 (6.8 to 3 ka BP)	U3 (2 ka BP to present-day)
Seismic unit volume	$2.723 * 10^8$ m^3	$1.677 * 10^8$ m^3	$1.511 * 10^8$ m^3
Annual sedimentation rate	$136.2 * 10^3$ m^3/y	$44.1 * 10^3$ m^3/y	$75.6 * 10^3$ m^3/y

In the model, sediment inputs from rivers and at oceanic borders are considered. However, only fluxes of fine suspended sediments in upstream rivers (Aulne, Elorn and Mignonne) are approximately known for the present-day and so human-influenced (section 2.2 and Tab. 4, scenario 4). Other studies have highlighted the potential climate-change impact on river discharge over the last 9 000 years (Fernane, 2014; Lambert, 2017; Penaud et al., 2020), but mainly qualitative information is available (section 2.2). No information is available for oceanic inputs, even for the present-day. Looking at available data and information from previous studies, the best solution is to modify river sediment supply in order to calibrate sediment inputs.

It is thus a calibration in three steps: (1) calibrate oceanic sediment supply with the present-day context (scenario 4), when the mean river discharges and concentrations of suspended matter are approximately known; (2) keep constant the availability of sediment along oceanic borders for past scenarios; and (3) modify the river water discharges for past scenarios, in order to obtain a similar annual sedimentation rate over the Bay as the one calculated from sediment data.

The calibration procedure for scenario 4 (step 1) and past scenarios (step 3) is as follow: First, a mass balance is made between the beginning and the end of the second year, for each grain-size class (over the same area as the available seismic coverage, see Fig. 3). Then all positive values are summed and the results are converted to volumes using the medium sediment density 1600 kg/m^3 (before any compaction or diagenesis processes, Tab. 5), and compare with the sedimentation rate calculated from sedimentary records (Tab. 3). In order to calibrate the sediment supply, a trial and error method is used, meaning that several two-year simulations are run until the annual simulated net deposition rate is close to the annual rate deduced from the preserved sedimentary unit volume.

(1) In fact, in the modelling frame, the sediment concentration for each class has to be set only when water entered the computational domain, while water exchanges at the open sea boundary were computed by the model, assuming no gradient of the flow component orthogonal to the boundary. Simulated sediment fluxes at the open sea boundary result from these “calibrated” concentrations and computed water fluxes.

(2) For the other three scenarios (1, 2 and 3), sediment availability is assumed to be constant at oceanic boundaries during the Holocene. The availability of sediment is assimilated to the mass in suspension within the sea boundary, which constitutes a strong assumption. This means that the suspended sediment concentration at the sea boundary has to be changed because, during the Holocene, the whole section of the sea boundary varied considerably, in relation with sea-level changes. Without any indication concerning bathymetric evolution on the continental shelf, bed elevation is assumed to be the same for all scenarii along the sea boundary, so that the average area of the sea boundary could be re-computed easily, for each scenario. The suspended sediment concentration of each sediment class at the oceanic boundary is deduced from the corresponding calibrated value for the present-day scenario, inversely proportional to the average section of the boundary (Tab. 4). Tidal currents are likely to vary simultaneously. The hydrodynamic model is expected to predict these changes, as the tidal forcing is assumed to be the same (Olivier et al., 2021).

(3) Then, the calibration of the three first scenarios is achieved by modifying river water discharge (and keeping their concentration in suspended matter) in order to obtain similar annual sedimentation rates for simulations and observations from seismic records, using the same type of comparison as in scenario 4. To avoid poorly parameterized annual variations for past river regimes, suspended matter and river water discharge are set as constant over the simulations. Mean values based on present-day data from DREAL Bretagne, are considered for all scenarios (Tab. 4, scenario 4). For scenarios 1, 2 and 3, a specific multiplicative factor is applied to the present-day mean water discharge of the rivers to obtain the same sedimentation rates as the one calculated from sedimentary records (Tabs. 4 and 5). For each simulation, the global volume of simulated deposits is therefore equivalent to the annual deposited (and preserved) volume of the corresponding sedimentary units: U1 (scenarios 1: 9 to 7.5 ka BP and 2: 7.5 to 7 ka BP), U2 (scenario 3: 6.8 to 3 ka BP), U3 (scenario 4: 3 ka BP to present-day, Tabs. 3 and 5). However, scenarios 1 and 2 are calibrated together as they represent the same sedimentary unit (U1), assuming a stronger river discharge during scenario 1 than in scenario 2. Their calibration (scenarios 1 and 2) results in the weighted average of both simulations, based on deposition chronology, compared to U1 annual sedimentation rate (Tabs. 3 and 5). The four calibrated simulations are presented in section 3.

Tab. 4: Hydro-sediment model forcing settings.

Scenario (Sc), river water discharge multiplicative factor (*x)	River water discharge ($m^3.s^{-1}$)			River suspended matter ($mg.l^{-1}$)			Oceanic border concentration ($mg.l^{-1}$)			
	Aulne	Elorn	Mignonne	Aulne	Elorn	Mignonne	mud	fine sand	sand	gravel
Sc 1*(10.9)	327	109	16,35	200	100	80	10.7	0,69	0,34	0,34
Sc 2*(4.0)	120	40	9	200	100	80	4,31	0,28	0,14	0,14
Sc 3*(2.0)	60	20	3	200	100	80	3,58	0,23	0,12	0,12
Sc 4*(1.0)	30	10	1,5	200	100	80	3,10	0,2	0,1	0,1

Tab. 5: Mass balance of gains and losses over 1 year of the four granulometric classes and the four scenarios (Sc). The balance is computed over an area of extension similar to seismic records (see Fig. 3).

Scenario (Sc)	mud (*10^6 kg/y)	fine sand (*10^6 kg/y)	sand (*10^6 kg/y)	gravel (*10^6 kg/y)	total (*10^6 kg/y)	Simulated sedimentation rate (*10^3 m^3/y)	Volume recorded (*10^3 m^3/y)
Sc 1	130	140	8.63	3.49	283	176.6	-

Sc 2	54.8	-7.74	-2.81	-1.65	54.8	34.2	-
Sc 1 + Sc 2 (U1)	-	-	-	-	-	141.0	136.2
Sc 3 (U2)	71.8	-29.6	-7.12	-3.17	71.8	44.9	44.1
Sc 4 (U3)	89.0	32.7	-0.56	-0.03	122	76.1	75.6

Note Tab. 5: sc 1 + sc 2 = Weighted average between scenario 1 (beginning of U1) and scenario 2 (end of U1) = (176.6 10^3*1500/2000) + (34.2*10^3*500/2000). Ponderation based on deposition chronology, i.e. beginning of U1 deposition: 9 to 7.5 ka BP and end of U1 deposition: 7.5 to 7 ka BP.*

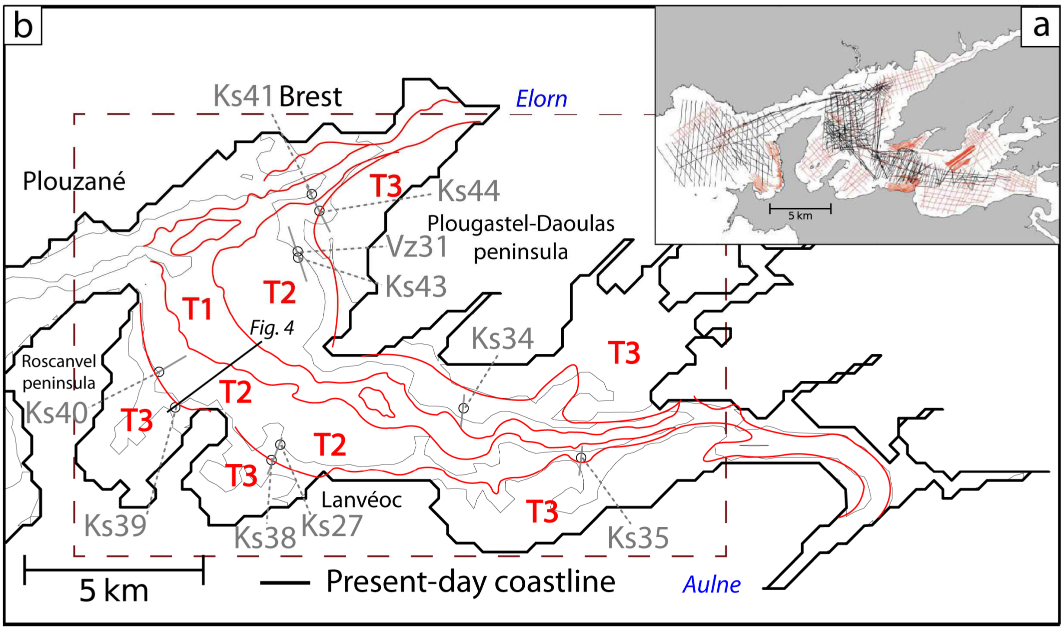

Fig. 3: (a) Location map of all seismic profiles used in this study (from Gregoire et al., 2017). (b) Location map of gravity-cores used in this study (sections 2.6. and 3.). Black line represents the seismic profile presented in section 2.6 and grey lines the seismic profiles available in supplementary material. The brown dashed rectangle is the area considered for mass balance calculation (Tab. 5).

2.6 Validation with sediment records

To overcome the lack of hydrodynamic data for past scenarios, simulation results were compared to observations from sedimentary cores and thickness maps for validation. Thickness maps provide the global distribution of preserved sediment deposits of each sedimentary unit, while core observations provide the deposit composition (grain size). For each scenario, a comparison is realized between the simulated bathymetric evolution and the thickness map of the corresponding sedimentary unit (section 3). This facilitates the comparison of simulated erosion and deposition trends with in-situ measurements. Information of ten cores (which have sampled the oldest sediment units) during the SERABEQ-03 campaign (Ehrhold and Gregoire, 2015) are also synthetised (Fig. 3 and Tab. 6) to compare and discuss the modeled grain-size distribution (see also supplementary material).

Tab. 6: Summary of core information and observations (cores from SERABEQ 3 Ehrhold and Gregoire, 2015)

Core label	Ks_27	Ks_34	Ks_35	Ks_38	Ks_39	ks_40	Ks_41	Ks_43	Ks_44	Vz_31

longitude		-4.4774	-4.3637	-4.4078	-4.4804	-4.5168	-4.5229	-4.4655	-4.4703	-4.4626	-4.4708
latitude		48.3032	48.2999	48.3126	48.2996	48.3128	48.3219	48.3662	48.3507	48.3620	48.3518
length (m)		1,68	2,64	3,31	3,52	3,55	3,57	2,14	3,6	3,31	2,64
Grain-size classes observed: M: muds; FS: fine sands; S: sands; G: gravels	U3	FS and S	M and FS	M and FS	M and FS	M and FS	S and G	FS and G	S	FS and S	FS
	U2	M	S	M and S	FS	M and S	-	M	-	M and FS	FS
	U1	-	M	M and FS	M	M	M	-	M	M and FS	-

However, the correlation between core and seismic/stratigraphic data are not straithforward. The identification of seismic units relies seismic geometries and facies rather than on shell dating, which is uncertain in estuaries because of the intense reworking induced by tide (*e.g.* Fig. 4 and all core-logs available in supplementary material). However, vertical resolutions between cores and seismic data are quite different, respectively centimetric and around 0.3 to 1 m. Observations from cores are simplified to correspond to the same grain-size classes as used in simulations: “mud” is for clay to silt and clay, “fine sand” is for silt to fine sand “sand” is for medium to coarse sands and larger grain size corresponds to “gravel” (Fig. 4 and Tab. 6). As our simulations aim to be representative of the main sediment dynamics over large time intervals, only preponderant grain-size classes are considered and not isolated variations, which are not representative of the main hydro-sediment dynamics trend induced by tide (and which are not simulated here) are not taking into account. This is why only the dominant and homogeneous part of deposits was considered. Cores can testify to the presence of one or two grain-size classes for each sedimentary unit. For example in core Ks_39, U1 consists mainly of mud and two small fine sand layers (Fig. 4). These two layers are not representative of U1 at this location and were therefore not taken into account for validation (Tab. 6).

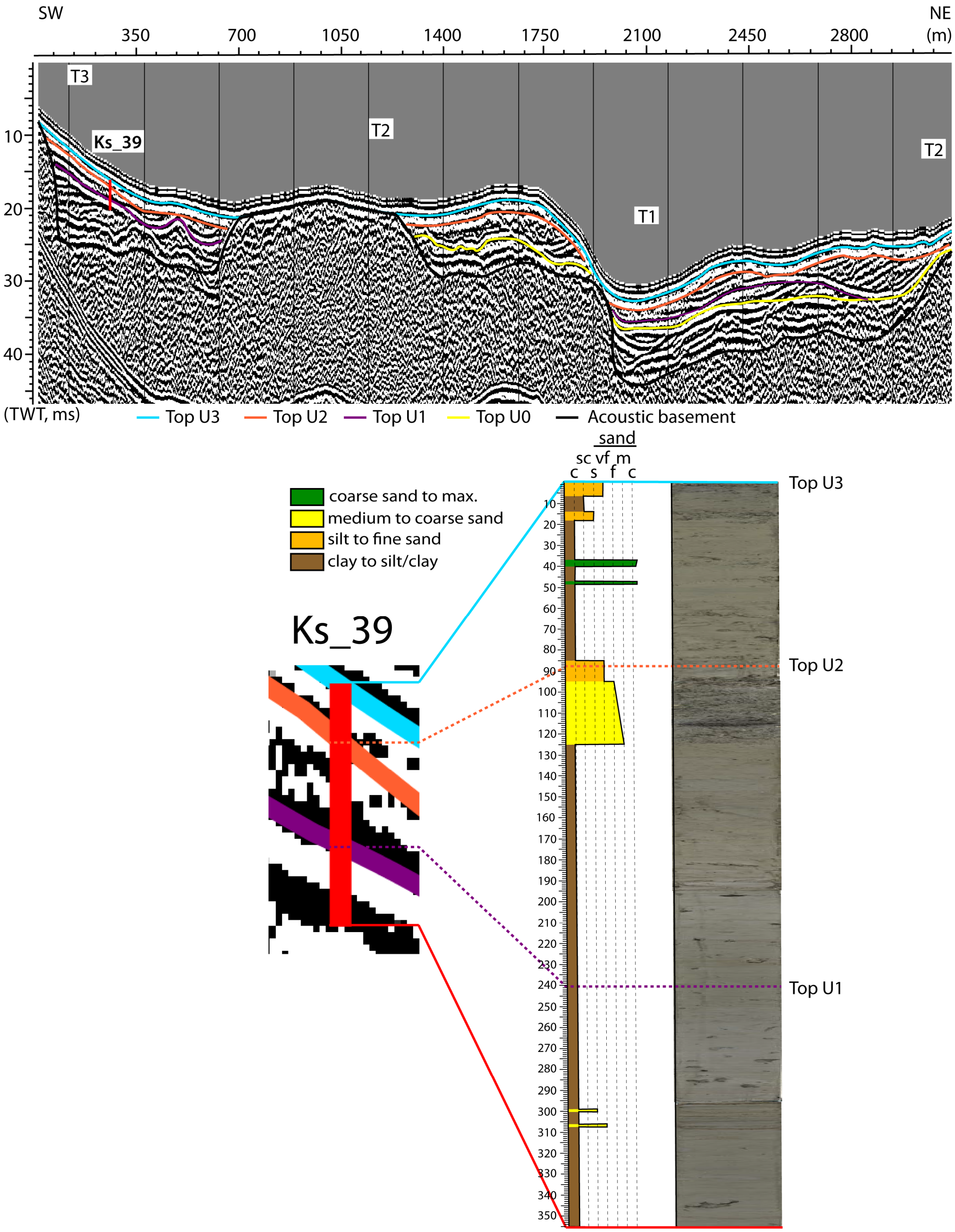

Fig. 4: (Top) Interpreted seismic profile (location on Fig. 3, profile 7). (Bottom) Photography and lithologic log for core Ks_39. c: clay, sc: silt and clay, s: silt, vf: very fine sand, f: fine sand, m: medium sand, c: coarse sand.

Note also that scenarios 1 (beginning of U1) and 2 (end of U1) represent two different dynamics for a single unit. Observed deposition of U1 may happen during scenarios 1, or 2, or both (*e.g.* Fig. 4). The same core observations are used for these two scenarios and are therefore validated together. This means that scenario 2 should explain the deposition observed in cores or must not show erosion if the corresponding grain-size classes were already deposited in scenario 1 (or less erosion than the quantity previously deposited).

3 Results

Outputs of simulations are described in this section in chronological order (from the oldest scenario to the youngest). The bathymetric evolution and distribution of mud and sands (*i.e.* fine sand, sand and gravel) are respectively compared to thickness maps and core observations.

3.1 Scenario 1: start of U1 (9 000-7 500 years BP)

The bathymetric evolution after one year of scenario 1 shows that most of the deposits are located over T2, over the widest parts of the main channel (T1) and, towards the Elorn river, T1 entirely undergoes sedimentation (maximum around 0.05 m, Fig. 5). Areas suffering erosion are only the narrowest parts of the main channel and rare locations of T2. The simulated bathymetric evolution and the thickness map of U1 only fit over T1 (Fig. 5). T3 is still continental during this first scenario and there is therefore no tidal deposition there. A substantial thickness is simulated over T2 during the beginning of U1, but none are preserved in sedimentary records (inset map of Fig. 5).

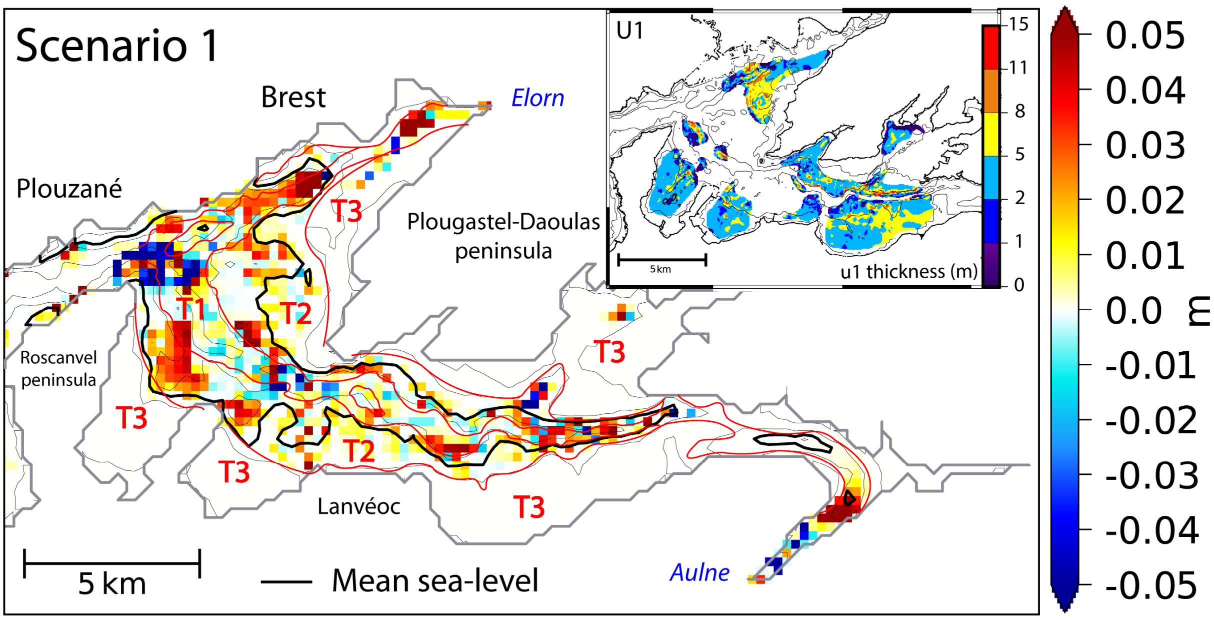

Fig. 5: Bathymetric evolution after 1 year for scenario 1 (9 k. BP). Red lines are morphological domain limits (T1, T2 T3) and the grey line is the present-day coastline. Black lines represent the mean sea-level (-26 m). The inset map is the thickness map of U1 modified from Olivier et al. (2021).

In scenario 1, mud is eroded from the entire subtidal zone (T1) and deposited on T2 terraces (intertidal, maximum around 30 kg/m², Fig. 6a). Sands erosion and deposition are mostly located over T1 (maximum deposition around 15 kg/m², Fig. 6b)

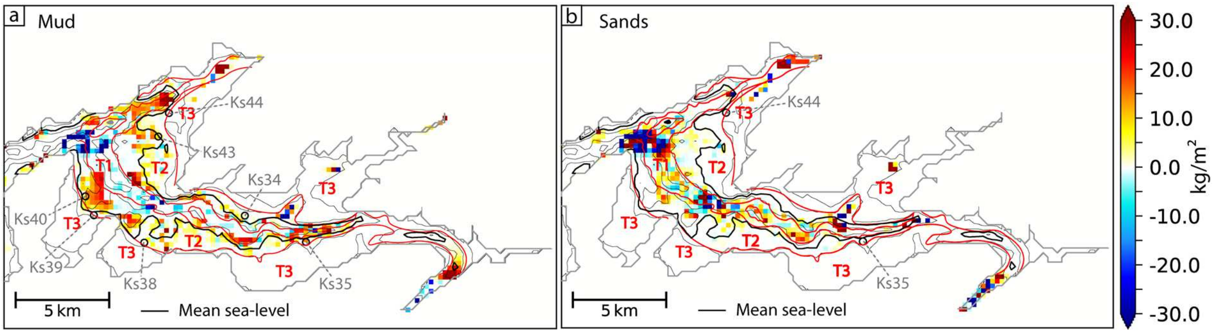

Fig. 6: Grain-size class erosion and deposition after 1 year for scenario 1 (9 ka BP): a mud, b sands (fine sand, sand, gravel). Black circles indicate locations where the corresponding grain-size class were recorded by cores. Core names are available in grey. Black lines represent the mean sea-level and red lines are morphological domain limits.

3.2 Scenario 2: end of U1 (7 500 – 7 000 years BP)

During scenario 2, the bathymetric evolution simulated is coherent with the thickness map of U1 (Fig. 7), with most of the deposits over T3, on slopes between T3 and T2 (maximum around 0.04 m, Fig. 7) and some accumulations located in the deepest parts of T1 (in the centre and to the north of the central area,). Most of T2 domain and T1 in the upper part do suffer erosion (maximum around -0.02 m over T2, Fig. 7).

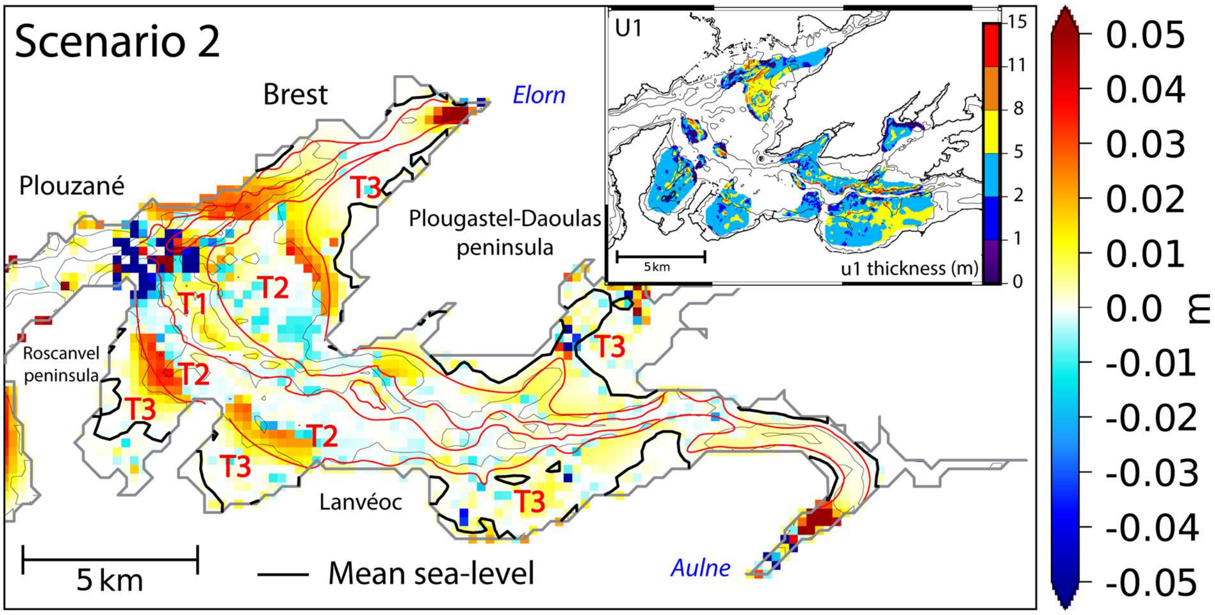

Fig. 7: Bathymetric evolution after 1 year for scenario 2 (7.5 ka BP). Red lines are morphological domains limits (T1, T2 T3) and grey line is the present-day coastline. Blacklines represent the mean sea-level (-10 m). The inset-map is the thickness of U1 modified from Olivier et al. (2021).

During scenario 2 (end of U1), mud deposits are simulated only over T3 and on slopes between T2 and T3 (between 5 and 20 kg/m², Fig. 8a). In the centre of the bay, non-cohesive sediments are remobilised mostly from T2 towards T1 and for fine sands also towards T3 (Fig. 8b). In the upper area, sands are transported more upward estuary than in the previous sceanrio (Fig. 8b).

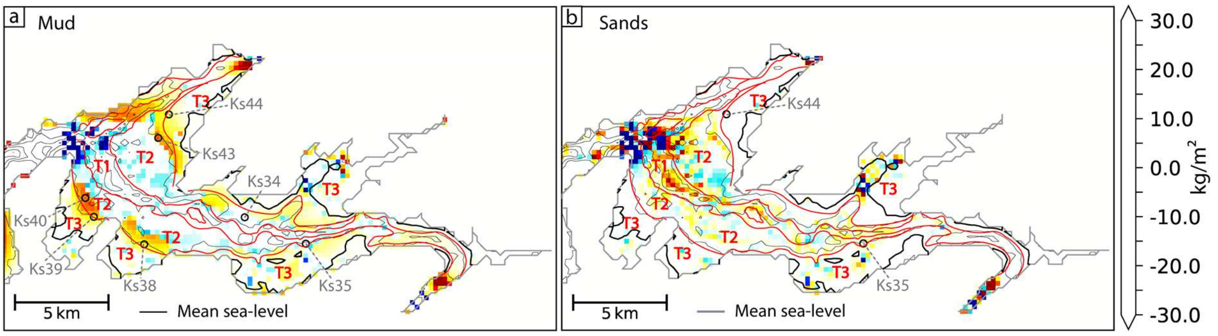

Fig. 8: Grain-size class erosion and deposition after 1 year for scenario 2 (7.5 ka BP): a mud, b sands (fine sand, sand, gravel). Black circles show where the corresponding grain-size class were recorded by cores. Core names are available in grey. Black lines represent the mean sea-level and red lines are morphological domain limits.

3.3 Scenario 3: U2 (6 800 – 3 000 years BP)

At this stage, erosion is mainly located over T2 in the central part and in the strait between Plougastel-Daoulas and Lanvéoc (maximum -0.03 m, Fig. 9). Simulated deposits are located over: T3, the slopes between T2 and T3 in the central area (maximum 0.04 m), and most of the upper area (T1 to T3, around 0.01 m, Fig. 9). The thickness map of U2 displays the same patterns: no deposit is preserved over T2 in the north of the main channel and the north of Lanvéoc, and accumulations are recorded over the rest of the Bay (inset map, Fig. 9).

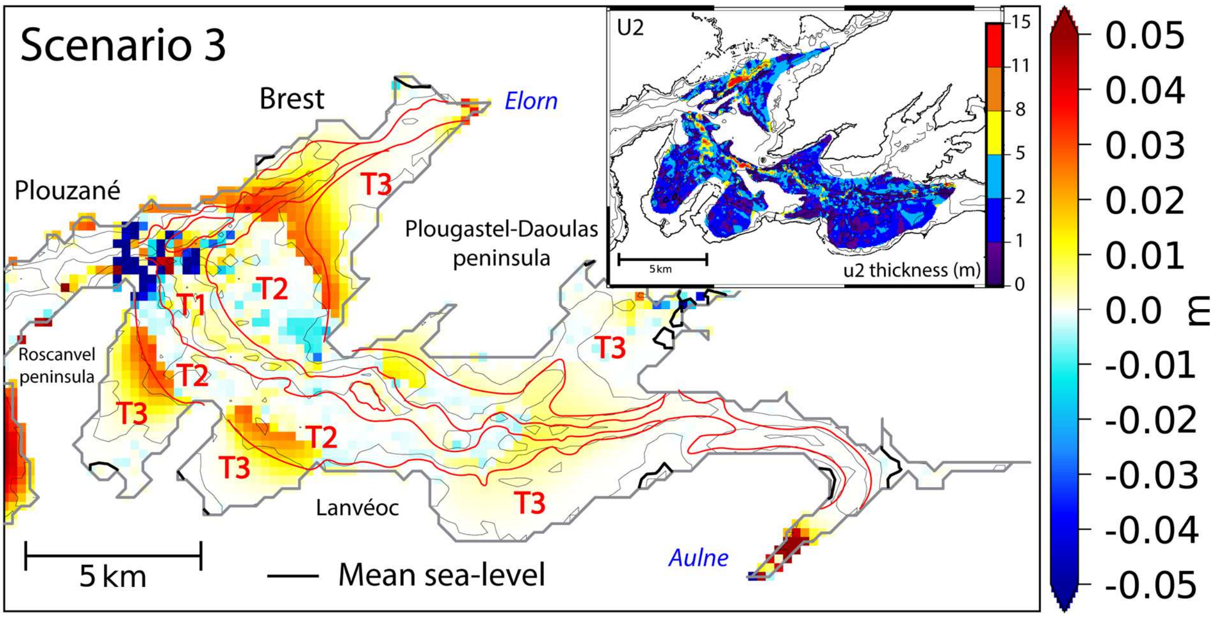

Fig. 9: Bathymetric evolution after 1 year for scenario 3 (6.8 ka BP). Red lines are morphological domain limits (T1, T2 T3) and the grey line is the present-day coastline. Blacklines represent the mean sea-level (-5 m). The inset map is the thickness of U2 modified from Olivier et al. (2021).

At 6 800 years BP, mud deposits are simulated over T3, on slopes between T2 and T3, and over most of the upper area (Fig. 10a). Sands erosion is simulated mostly over T2 and deposition is simulated at the edges of the same morphological domain: on slopes between T2 and T3 (5 to 10 kg/m², Fig. 10b) and T1 (around 15 kg/m², Fig. 10b).

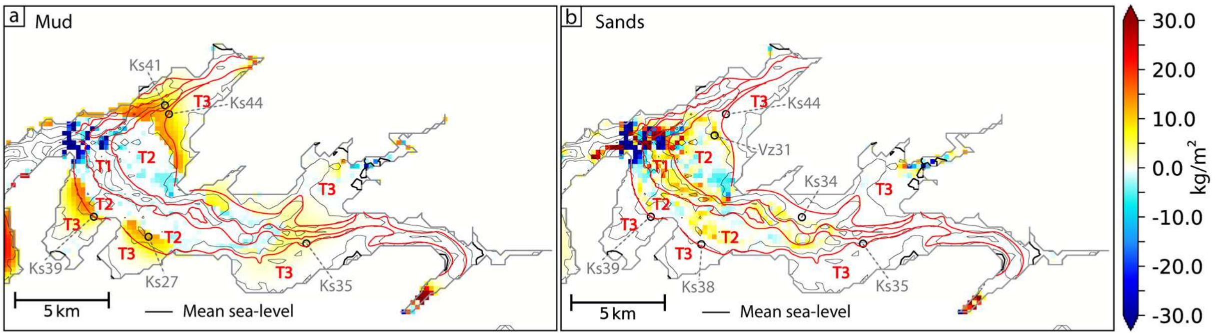

Fig. 10: Grain-size class erosion and deposition after 1 year for scenario 3 (6.8 ka BP): a mud, b sands (fine sand, sand, gravel). Black circles show where the corresponding grain-size classes were recorded by cores. Core names are available in grey. Black lines represent the mean sea-level and red lines are morphological domain limits.

3.4 Scenario 4: U3 (2 000 years BP - Present-day)

During scenario 4, erosion patterns are mainly located over T2 (maximum -0.04 m, Fig. 11), over T1 in the upper part and towards the mouth of the Aulne river (<-0.01 m). Depositional areas are over T3 (maximum 0.04 m, Fig. 11) and T1 in the centre (maximum 0.05 m, Fig. 11). Important deposits are also simulated on slopes between T3 and T2 West of Lanvéoc (maximum 0.03 m, Fig. 11). There is one major difference between the bathymetric evolution simulated and the thickness map of U3: simulated deposits are located mostly over T1 and T3 in the centre (Fig. 11) whereas seismic data interpretation describes some deposits also over T2 (inset map, Fig. 11).

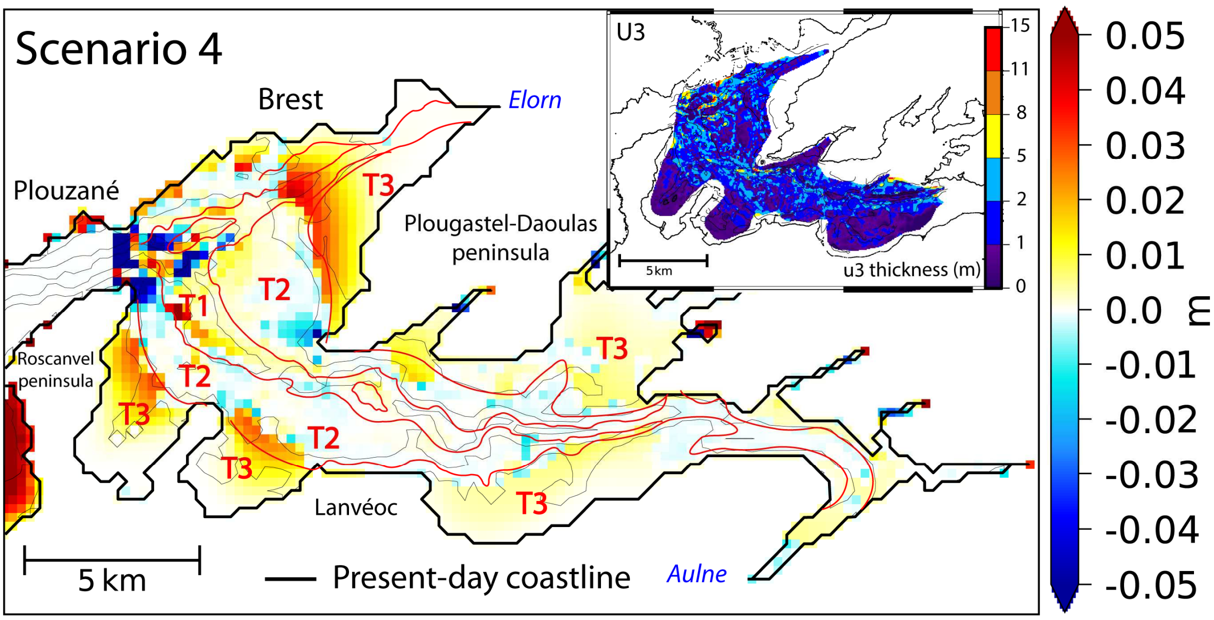

Fig. 11: Bathymetric evolution after 1 year for scenario 4 (present-day). Red lines are morphological domain limits (T1, T2 T3) and the black line is the present-day coastline. The inset map is the thickness of U3 modified from Olivier et al. (2021).

During U3, cohesive sediments settle mostly over T3 (around 1 to 15 kg/m², Fig. 12a) and sands at the edges of T2 domains (T1 mostly and slopes between T2 and T3, maximum > 30 kg/m², Fig. 12b).

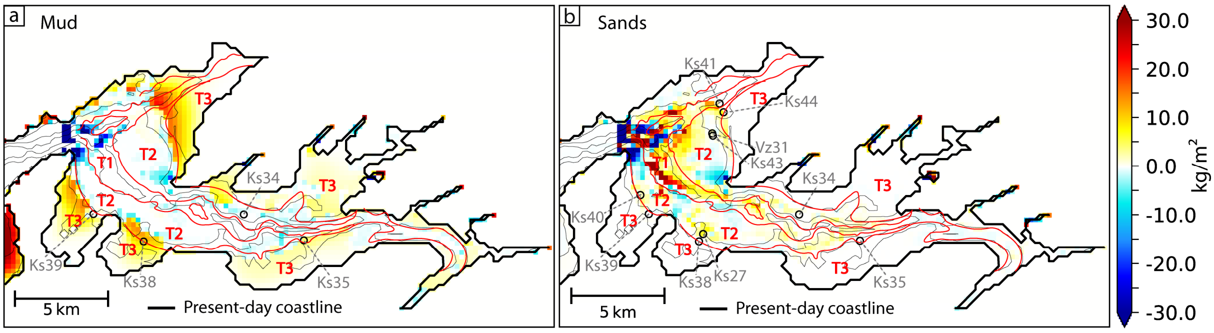

Fig. 12: Grain-size class erosion and deposition after 1 year for scenario 4 (present-day): a mud, b sands (fine sand, sand, gravel). Black circles show where the corresponding grain-size classes were recorded by cores. Core names are available in grey and red lines are morphological domain limits.

3.5 Holocene reconstruction

The four scenarios enable a reconstruction of hydro-sediment pattern evolution over the last 9 ka. At the beginning of U1 deposit (9 ka BP) sea-level is 26 metres lower than present-day level (intertidal area over T2 terraces). Main deposition takes place over T2 and within the main channel in the upper zone (Figs. 13a and 13b). Then, at the end of U1 deposition (7.5 ka BP), sea-level reaches 10 metres below present-day level, shifting the intertidal area from T2 (scenario 1) to T3 (scenario 2). Bottom current velocities over T1 decrease with increasing depth and the highest velocities are then observed over T2 (Olivier et al., 2021 and supplementary materials). Tidal currents no longer follow the shape of the main channel in the central area. The distribution of main currents is largely influenced by strait morphology in the east (ebb) and west (flood) of the central area, which orientates water fluxes (Olivier et al., 2021). This results in the formation of a clockwise gyre in the centre of the bay. Tidal currents induce strong erosion of the initial sediment layer (especially mud): a substantial part of sediments deposited during scenario 1 is reworked (over T2 and T1 towards the Aulne mouth, Figs. 13a to 13d). The sediment dynamic simulated for scenario 2 explains the absence of most of scenario 1 deposits from sedimentary records. The beginning of U1 (scenario 1: 9 to 7.5 ka BP) is almost not preserved, except over T1 and mud deposits over slopes between T2 and T3 in the centre of the Bay. Sedimentation during scenario 2 mainly occurs over T3 (mud), in the centre of the bay over the slopes between T2 and T3 (mud and fine sand) and over T1 (fine sand and sand, Figs. 8, 13c and 13d). The simulated bathymetric evolutions of scenarios 1 and 2 are consistent with U1 thickness map, in the same way as the distribution of grain-size classes with core observations. This demonstrates that sedimentary records of U1 mainly testify to the end of U1 hydro-sediment dynamic (scenario 2: 7.5 to 7 ka BP). The beginning (scenario 1: 9 to 7.5 ka BP) is almost unpreserved (Fig. 13a to 13d).

U2 deposition takes place between 6.8 and 3 ka BP (scenario 3) with sea-level five meters below the present-day level. An important part of the T3 terraces are then located in a subtidal domain and ebb and flood tide distributions are different in the upper area (ebb on T3 and flood on T1, Olivier et al., 2021). Simulation outputs and sedimentary records (thickness map and cores) display the same trends throughout the Bay: main sedimentation over T3, the slopes between T2 and T3, T1 in the centre (Fig.

13e), and over most of the upper area (Fig. 13f). Between U1 and U2 the hydro-sediment patterns are similar in the centre, but very different in the upper zone (Fig. 13d and 13f). Between scenarios 2 and 3 sea-level rises by five metres, resulting in most T3 terraces in subtidal domain. The subtidal area increases substantially in comparison to the amplitude of sea-level rise (Fig. 15e). The active flow section width (*i.e.* the section on which incoming and outgoing water to/from upstream areas flow) increases greatly, (only T1 and T2 in scenario 2, and T1, T2 and T3 in scenario 3). This results in weaker currents in the upper area than in the previous scenario (end of U1, Olivier et al., 2021) and it allows the deposition of mud in all morphological domains in the upper area (Fig. 13f). However, we observe a difference of maximum sediment rate between simulations and sedimentary records over T1 and T3 in the centre: the largest sediment thicknesses observed are located over T1 (Fig. 13e), but the largest thicknesses simulated are over T3 and over the slopes between T2 and T3 (Fig. 13e). In the centre (T1 and T2), deposits are made mostly of sands (without mud), while over T3, deposits are mainly mud (Fig. 10). This suggests that during U2 deposition, larger volumes of sands, and a smaller volume of mud were available than during U1 deposition (scenarios 1 and 2). Sediment supply probably changed between U1 and U2. This hypothesis is supported by the good correlation between erosion/deposition patterns simulated and sedimentary records (Figs. 9 and 10), but further simulations would be needed to confirm sediment supply evolution.

During the deposition of U3 (scenario 4), T3 terraces are subtidal and only a few intertidal areas are observed within the Bay of Brest. Between scenario 3 and 4, sea-level rises by five metres, while the subtidal area in the Bay remains similar (new subtidal areas are mainly located in upstream part of the estuary and close to the rivers mouths, especially the Aulne one). The active flow section width remains similar and the water volume transported by the tide through the active flow section increases. More intense currents characterise the upper area compared to scenario 3 (Olivier et al., 2021). During scenario 4, currents prevent mud deposits over T1 domain in the upper area, which was covered by mud during scenario 3 (Figs. 10a and 12a). The bathymetric evolution of scenario 4 and the thickness map of U3 are consistent over the upper area (Fig. 13h) and over T1 and T3 in the centre (Fig. 13g). However, the thickness map displays U3 deposits over T2 in the centre, where few deposit are simulated (Figs. 11 and 13g). The hydro-sediment dynamic simulated over T2 remains unchanged from scenario 2 to 4 in the centre (7 500 years BP, gyre formation): muds are removed from T2 and T1 towards T3 and non-cohesive grain-size classes are mostly transported over T2. This suggests that the sediment deposits interpreted for U3 over T2, could be non-cohesive sediments frequently reworked over the last 7 500 years. This hypothesis is supported by present-day grain-size classes and sediment structure distribution maps (Gregoire et al., 2016), which reveal that T2 terraces in the centre are either mostly covered with coarse sediments, or not covered, and many active sediment structures have been identified over the same area (*e.g.* sand ridges, comet tails). Taking into account the simulated dynamics (scenarios 2, 3 and 4) and observations from Gregoire (2016), sediment thickness (ranging from 1 to 5 m) over T2 terraces (U3, Figs. 11 and 13g) probably correspond to non-cohesive sediments reworked over the last 7 500 years.

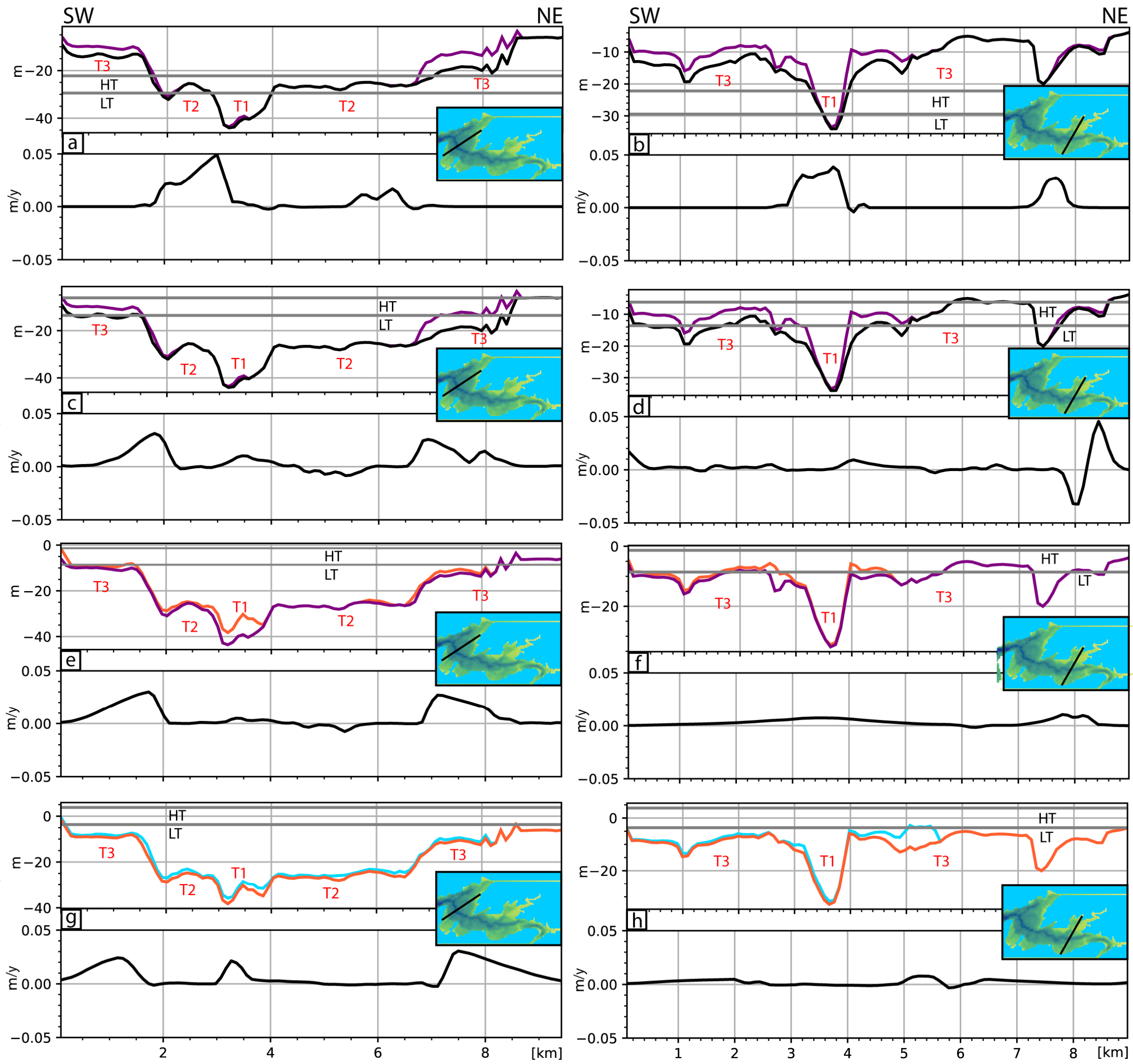

Fig. 13: Cross-section of sedimentary unit thicknesses (black line top of U0, purple line top of U1, orange line top of U2 and blue line top of U3, vertical reference: present-day sea-level) compared to simulated bathymetric evolution over 1 year, (left) in the central area (a: scenario 1, c: scenario 2, e: scenario 3, and g: scenario 4) and (right) in the upper area (b: scenario 1, d: scenario 2, f: scenario 3, and h: scenario 4). Inset maps show the locations of cross-sections. Grey lines represent the highest free surface level (HT: Highest Tide) and the lowest free surface level (LT: Lowest Tide).

4 Discussion

4.1 Impact of sediment sources (boundary condition)

The parameterisation of past sediment supply is a challenge, given the number of unknown parameters. However, the impact of different sediment sources is one of the most important issues in understanding coastal basins. To assess the influence of sediment sources in the Bay of Brest, two additional simulations are performed for each scenario. They have the same parameterisation as simulations presented in section 2, but without the initial sediment layer. The four scenarios are simulated either without river input, or without input from oceanic borders. The aim of this sensitivity exercise is to explore the impact of continental and oceanic sources, in terms of amount and distribution of sediment supply within the Bay. Results for scenarios 1 and 4 with a single type of input are presented in Fig.14.

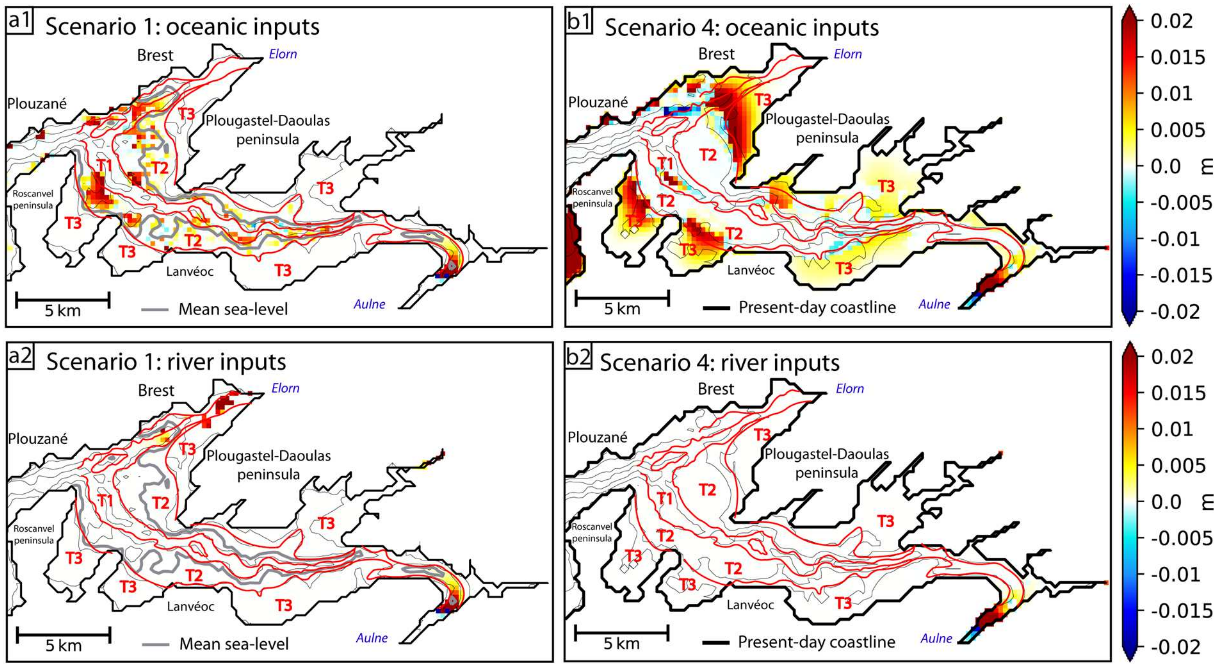

Fig. 14: Simulated bathymetric evolution of the Bay of Brest after one year. a1: Scenario 1 without initial sediment and without river water discharge. b1: Scenario 4 without initial sediment and without river water discharge. a2: Scenario 1 without initial sediment and without oceanic border input. b2: Scenario 4 without initial sediment and without oceanic border input.

The sedimentation induced by river sediment inputs is mainly concentrated in channels close to the Elorn and Aulne mouths (Figs. 14a2 and 14b2), while the sedimentation induced by oceanic sediment inputs is distributed throughout the Bay (Figs. 14a1 and 14b1) and in greater quantities for both scenarios 1 and 4. The same observations are made for scenarios 2 and 3 and thus only scenarios 1 and 4 are displayed (Fig. 14). Simulations with only oceanic inputs display the same global deposition pattern as the genuine scenarios that were parametrized with an initial sediment layer in the Bay and river inputs (section 3, Figs. 5 and 11, to compare with Figs. 14a1, 14b1).

In order to quantify the impact of sediment sources, the annual amount of sediment deposited is calculated over the Bay and rivers (*i.e.* from the strait between Plouzané and Roscanvel peninsula to the rivers/land boundaries). Total deposited masses are estimated from simulations without river and from simulations without oceanic inputs (for each scenario) to be compared in order to give an approximation of the respective influences of sediment sources on simulation. Oceanic and river inputs respectively represent 65%, and 35% of the quantity deposited during both simulations for scenario 1. Their respective influences are 80% and 20% for scenario 2, 89% and 11% for scenario 3, 91% and 9% for scenario 4. The supply progressively decreases during the Holocene, probably in relation with the evolution of the multiplicative factor used on river fluxes between scenarios. The weighted average of sediment quantity deposited along the deposition time interval of the three units (Fig. 2) shows that oceanic inputs represent about 84% of sediment supply during the Holocene (9 ka BP - present-day), against 16% for river inputs. These tests show that net sedimentation in the Bay of Brest mainly depends on oceanic inputs, which is an unexpected result and goes against what is suggested in previous studies using sediment records (section 2.2, Grégoire, 2016).

However, the methodology used for the calibration of sediment supply implies some approximation. Oceanic inputs are unknown, even now, and have been calibrated in order to fit the average sedimentation rate at present-day, with a crude approximation of river inputs (scenario 4). Regarding past scenarios, it has been assumed that the sediment availability, arbitrarily defined as the quantity in suspension (mostly mud and fine sand) along the oceanic boundary, remained constant over the Holocene. This hypothesis implies changes in net fluxes to the Bay of Brest, accounting for changes in depths on the continental shelf (known, as they mainly result from sea-level rise) and tidal flow variations which can be fairly computed by the model. In addition, the initial calibration concerns the sum of all types of sediment, without considering any sensitivity to changes in gravel/sand/fine sand/mud ratios. Last, sediment processes simulated between oceanic boundaries and the entrance of the Bay of Brest have not been analysed, nor their possible evolution through the Holocene. The overall uncertainty on the actual net fluxes at the open boundary remains very high, and hypotheses are debatable. Then past river inputs have been fitted until the average net sedimentation rate observed in seismic records could be simulated through the three modelled scenarios. This led to a strong decrease of river fluxes over the Holocene (about a factor 10) which is neither confirmed nor infirmed by our knowledge on climate and hydrology evolutions (section 2.2). The choice of correcting river discharges and not the suspended sediment concentration was made for numerical reasons, as a too high concentration cannot be transported to the Bay by the present-day river water discharge. Anyway, changes in river water fluxes had very limited impact on hydrodynamic patterns in the Bay (see supplementary material and Olivier et al., 2021). The main uncertainty of the calibration strategy is so related to the sediment rate calculated from sedimentary units: it corresponds to a preserved sediment volume, and so to a minimum estimate of sediment budget that not includes explicitly the possible remobilization, which is still unknow).

This sensitivity exercise demonstrates the importance of better understanding and measuring sediment availability on the continental shelf, which can play a major role in coastal basin infilling. The balance between sediment sources has a strong influence for estuary infilling and yet sediment supply stills an important unknown for past reconstructions (same observation for the Humber estuary, Rees et al., 2000; Townend et al., 2007).

4.2 Long-term evolution of deposition and erosion patterns

Modelling over four scenarios highlighted that at the time scale of the Holocene transgression, boundaries between erosion and deposition, as well as sand/mud transition, are progressively pushed upstream the estuary (*i.e.* on flanks and in the direction of the river mouth) because of tidal asymmetry in the Bay of Brest (see supplementary material); this is also visible through the grain-size increase in deposits observed from cores located on the slopes between T2 and T3 domains (Tab. 6). However, the progression of these boundaries upwards of the estuary does not strictly correspond to sea-level rise. As an illustration of these considerations, Figure 15 aims to display the evolution of depositional areas and the interpreted preservation of deposits, in relation to paleoenvironmental changes.

At 9 ka BP (-26 m), most of non-cohesive sediments are transported over T1 and cohesive sediments settle in intertidal areas (T2 terraces) and over T1 towards river mouths (Fig. 15a and 15e).

At 7.5 ka BP (-10 m), most sands movements take place over T2 and they settle at the edges of T2 terraces (over T1 or on slopes between T2 and T3, Fig. 15b). In the upper area, T1 remains the only subtidal domain (as T2 is small in this region, Fig. 15e). Thus, the upstream tidal prism increases substantially (water volume transported by the tide through the upper area), while the active flow section remains of similar width (only T1). Intense tidal currents are observed over T1 and sands are transported over the same morphological domain and secondary channels (Fig. 15b). Previous muddy deposits (9 ka BP) are removed from T2 in the centre and from T1 in the upper area towards T3 terraces (Fig. 15b).

At 6.8 ka BP (-5m), patterns similar to the previous scenario are observed in the centre. In the upper area, the active flow section width increases substantially (T3 subtidal, Fig. 15e). This fast and important increase in the active flow section width induces less intense currents in the upper area than during the previous scenario (Olivier et al., 2021), as a slightly greater volume of water is transported by tide through a much larger section. This phenomenon is amplified by the shallow depth and flat shape of T3, which induces strong friction all over this morphological domain at 6.8 ka BP. This allows the deposition of mud over all the morphological domains and only a few sands are transported by tidal currents into the upper area (Fig. 15c).

At the present-day, the limit between mud and sands deposits is located further towards T3 than during the two previous scenarios in the centre, but general patterns are the same since 7.5 ka BP (Fig. 15a, 15b, 15c). The active flow section in the upper area remains of similar width, while the upstream tidal prism still increases (Fig. 15e). Thus, higher currents characterize the upper area of the estuary than at 6.8 ka BP (Olivier et al., 2021). The augmentation of tidal current velocity is amplified by the reduction of friction over T3 with the increasing depth (Fig. 15e). Non-cohesive sediments are transported more upward over the main channel than during the previous period and muds settle only over T3 (Figs. 15c and 15d).

These observations are in agreement with the study of Guo et al. (2022), who simulated the evolution of conceptual estuaries over 100 years with different widths of terraces bordering a main channel. They showed that, when these terraces are narrow, deposition is concentrated more upstream than when terraces are large. Tidal dynamic is closely dependent on the underlying morphology and therefore changes through time. In the Bay of Brest, large and fast coastline retreats are mainly perpendicular to the main channel (T1), generating a strong increase in the active flow section width when terraces (T2 and T3) pass into subtidal domain. Upstream areas of the Bay are characterized by steep banks rivers. It implies a large variation of accommodation space between scenarios (Fig. 15e and Gregoire et al. 2017). Bottom morphology and the coastline (shape and nature) both affect tidal flows and sediment distribution. Different estuary shapes and embankments will induce a different evolution of hydro-sediment pattern in relation to sea-level rise (Townend et al., 2021; Guo et al., 2022).

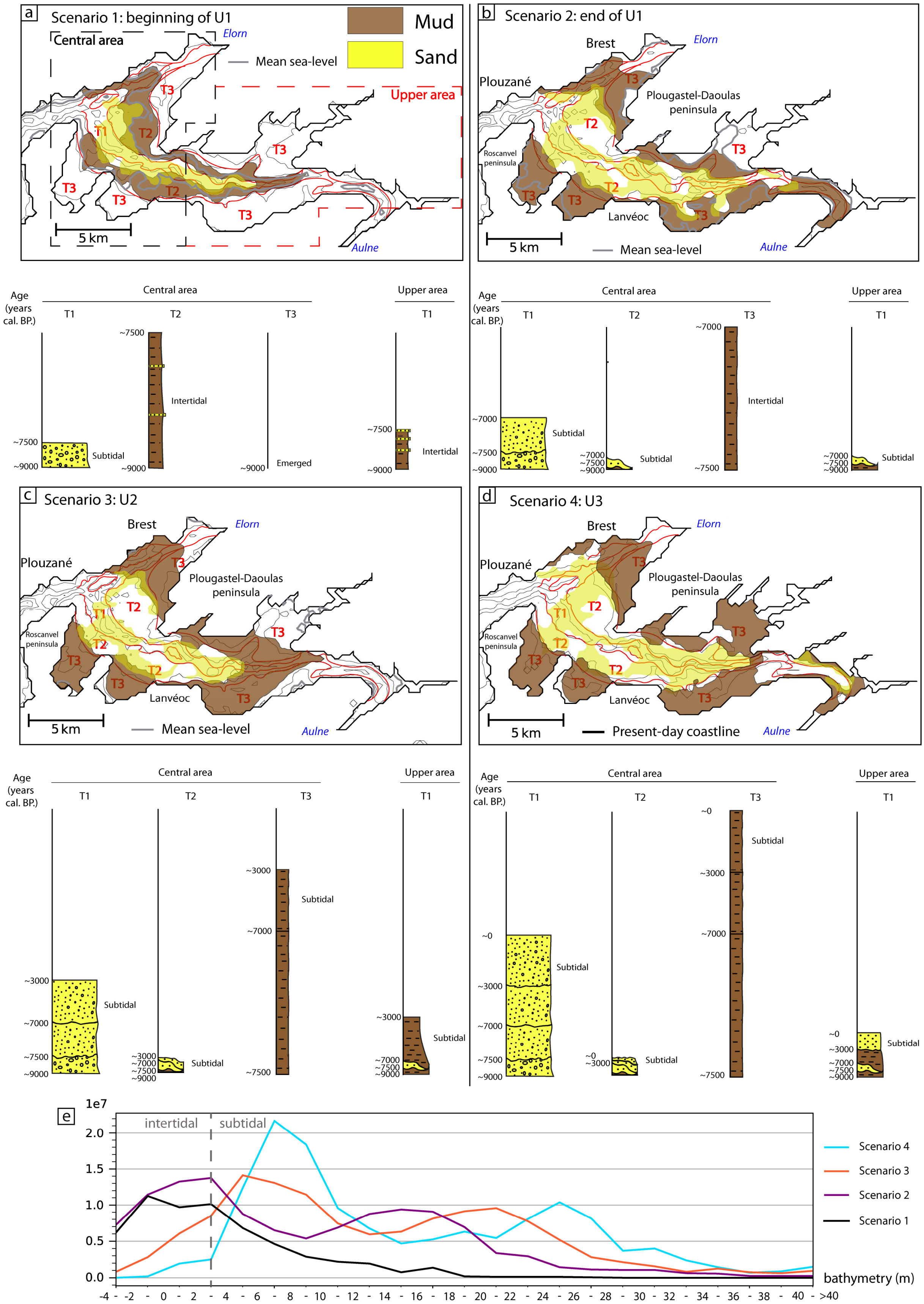

733

734 *Fig. 15: Schematic representation of deposition patterns along the Holocene. For each scenario (a, b, c, d) maps represent*
735 *the deposition area of mud (brown) and sand (yellow) from modelling results, and four synthetic logs display the theoretical*
736 *stratigraphic stacking of each morphological domain at the end of simulated scenario (the vertical scale respects*

representative thicknesses for each morphological domain). e: the hypsometry of each scenario over the Bay of Brest (vertical reference: mean sea-level of each scenario).

These qualitative observations are displayed over the simplified upper zone of the Bay of Brest, to highlight the main mechanisms and triggers of hydro-sediment changes (Fig. 16). It gives a general understanding of the hydro-sedimentary response of an estuary to sea-level changes and could therefore help to interpret sediment records elsewhere. They illustrate that the limit between erosion and deposition, or the transition between sandy and muddy deposits, do not necessarily move upward the estuary during transgression cycles (as classical sequence stratigraphic interpretations suggest). For estuaries displaying seafloor morphology with a main channel(s) surrounded by different levels of terraces (*e.g.* morphology inherited from a fluvial paleo-system), those boundaries move upward or downward the estuary depending on the ratio between the variations of the active flow section width and the increase of total water flux (*i.e.* the tidal prism, upstream the considered section). If sea-level rises and the active flow section remains of similar width, a greater water volume passes through a similar section and tidal current velocities increase (Fig. 15, difference between scenarios 1 and 2; Fig. 16, between steps 1 and 2, or between 3 and 4). In this case the transition between erosion and deposition, as well as between cohesive and non-cohesive sediment deposition moves upward the estuary. When the active flow section width increases rapidly, for instance in the case a flat transversal terrace is inundated, the same (moderate) increase of upstream tidal prism is likely to flow through a much larger section, inducing a decrease in tidal current velocities. In this case, mud and sand deposition boundaries move downward the estuary (Fig. 15, between scenario 2 and 3; Fig 16, between step 2 and 3). It can be noted that the distinction between active and passive sections depends on the relative depth of shallow sectors: in case of juxtaposition of channels and intertidal areas, the latter are likely to few contribute to the flow. When sea level rises, the intertidal zone becomes subtidal, with relative low velocities at the beginning, because of strong bottom friction when depths are small, but with larger velocities all the more depths increase.

The main factors controlling the location of mud and sand deposits over long time scale are therefore the upstream tidal prism (volume of water transported by the tide) and the active flow section width. A different evolution is expected for different configurations and upstream morphologies, but those observations should be helpful for many other estuaries with similar morphological domains.

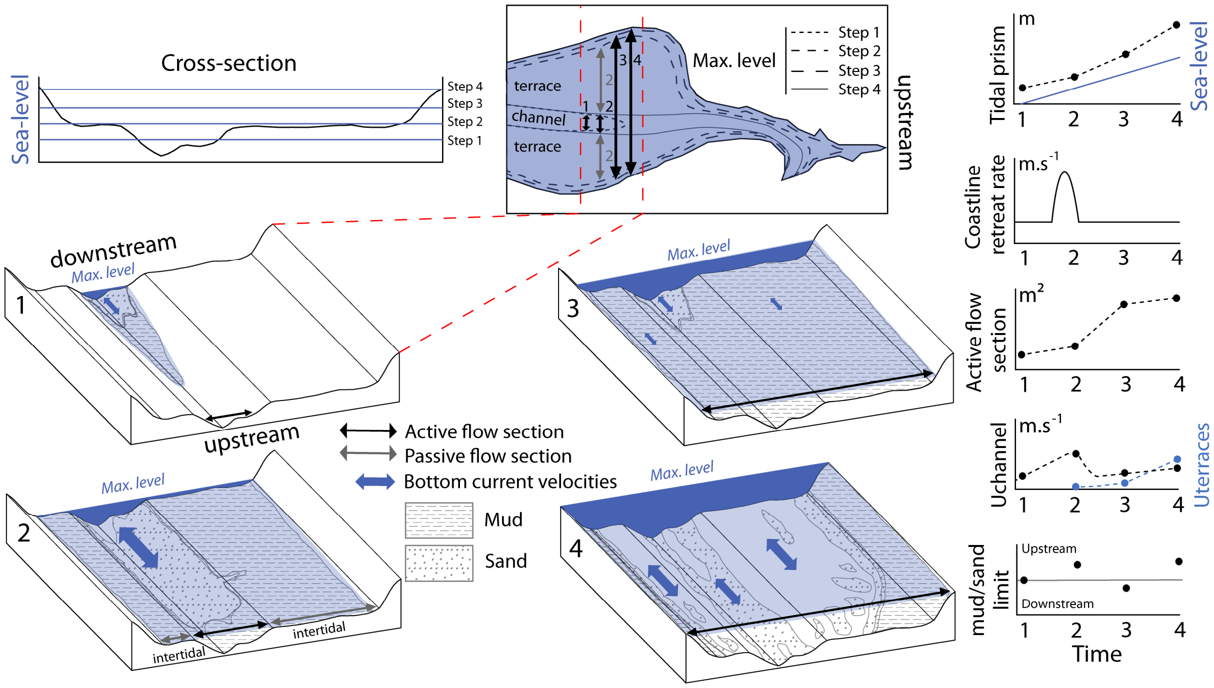

Fig. 16: Conceptual 3D diagrams of the evolution of mud and sand distributions over a typical estuarine domain constituted of one channel and one level of terraces, during a transgression with a constant rate of sea-level rise. The blue area represents the maximum sea-level elevation and blue arrows represent the relative main velocities of ebb and flood tides bottom currents. The active flow section width is represented by black arrows.

We are thus able to propose a schematic conceptual model of the impact of flooding of terraces on the evolution of depositional areas within an estuary (Fig. 16). Observations are in line with the global sediment and grain-size distribution of Davis and Dalrymple (2012): the most energetic zone is composed of non-cohesive sediments, that form sediment structures (*e.g.* sand ridges, comet tails); towards shallower parts of the estuary (flanks and river mouths) deposits are finer (mix of mud and fine sand); and towards the shallowest area to the coastline, deposits are only muddy (Fig. 15). This study also demonstrates that erosion/deposition and the cohesive/non-cohesive boundaries cannot be related to a depth threshold, but vary with the distribution of tidal currents. The distribution of tidal currents is primarily function of the shape of the basin (seafloor morphology and sea-level height), but locally the shape of the coastline may be the most significant parameter. For example, straits can expose some morphological domains to strong tidal currents (*e.g.* T2, in the centre, Olivier et al., 2021). Conversely coves and bays can be protected from strong currents, such as T3 terraces within the Bay of Brest, which are favourable to mud accumulation from +3 m to -15 m (depth relative to present-day mean sea level, scenarios 2 to 4, Fig. 15).

5 Conclusion

This paper aims to explore the impact of tides on the evolution of sediment dynamics over the Holocene in the Bay of Brest. To understand the infill of this estuary, seismic profiles and cores are available and led to a previous interpretation of sediment records (Grégoire et al., 2017). Thanks to seismic stratigraphy correlated with cores facies and dating, Gregoire et al. (2017) interpreted distinct sedimentation periods.

This paper proposes an interdisciplinary methodology to explore the impact of tides on sedimentary deposits at geological timescale (9 ka). Following previous sediment records interpretation, each key paleoenvironment of the Bay of Brest Holocene infilling (seafloor and sea level) are rebuilt. Simulations are thus representative of larger periods than the one simulated. This hypothesis allows the comparison between simulations and sediment records. Previous work has led to the reconstruction of tidal circulations during these key moments, by using a hydrodynamic model (Olivier et al., 2021). This study focuses on the hydro-sedimentary response of the estuary to long-term paleoenvironmental evolution by using a hydro-sediment model MARS3D-MUSTANG.

Four scenarios are simulated to reconstruct main sedimentation periods (spatial distribution and nature of the deposits). A fairly coherent result is obtained, allowing to explain the preserved sediment records, taking into account successive periods of deposition and erosion, linked to the evolution of tidal currents. Even if, the simulation results are very sensitive to sediment sources calibration, it appears that marine inputs dominate the sediment deposited over the Holocene.

Simulation results highlight also that movements of the limits erosion / sand deposition / mud deposition between scenarios are mainly linked to the evolution of the tidal prism and the active flow section width over long-term intervals: when fast and significant expansion of the active-flow section width occurs, those boundaries move down-estuary, while the opposite occurs when the increase of active-flow section width remains low during sea-level rise. During a transgression, seafloor morphology is of an uppermost important for the evolution of the active flow section and the tidal prism. Different evolutions of erosion and deposition limits are expected for different estuaries morphologies. However, the morphology of the Bay of Brest (*i.e.* incised valley surrounded by terraces) is very common and those observations could help to understand sediment records of other estuaries dominated by tides.

References

Bárcena, J.F., García-Alba, J., García, A., Álvarez, C., 2016. Analysis of stratification patterns in river-influenced mesotidal and macrotidal estuaries using 3D hydrodynamic modelling and K-means clustering. Estuarine, Coastal and Shelf Science 181, 1–13.

Berger, A., Loutre, M.F., 1991. Insolation values for the climate of the last 10 million years. Quaternary Science Reviews 10, 297–317. https://doi.org/10.1016/0277-3791(91)90033-Q.

Beudin, A., 2014. Dynamique et échanges sédimentaires en rade de Brest impactés par l'invasion de crépidules, 224 pp.

Bjune, A.E., Bakke, J., Nesje, A., and Birks, H., 2005. Holocene mean July temperature and winter precipitation in western Norvay inferred from palynological and glaciological lake-sediment proxies. The Holocene 15,2, 177–189.

Bolla Pittaluga, M., Tambroni, N., Canestrelli, A., Slingerland, R., Lanzoni, S., Seminara, G., 2015. Where river and tide meet: The morphodynamic equilibrium of alluvial estuaries. J. Geophys. Res. Earth Surf. 120, 75–94. https://doi.org/10.1002/2014JF003233.

Braat, L., van Kessel, T., Leuven, J.R.F.W., Kleinhans, M.G., 2017. Effects of mud supply on large-scale estuary morphology and development over centuries to millennia. Earth Surf. Dynam. 5, 617–652. https://doi.org/10.5194/esurf-5-617-2017.

Chataigner, T., 2018. Modélisation de la dynamique sédimentaire en rade de Brest, intégrant une résolution spatiale des fonds plus fine que celle de la masse d'eau.: Master report, University of Occidental Brittany, 36p.

Coco, G., Zhou, Z., van Maanen, B., Olabarrieta, M., Tinoco, R., Townend, I., 2013. Morphodynamics of tidal networks: Advances and challenges. Marine Geology 346, 1–16. https://doi.org/10.1016/j.margeo.2013.08.005.

Collins, D.S., Avdis, A., Allison, P.A., Johnson, H.D., Hill, J., Piggott, M.D., 2018. Controls on tidal sedimentation and preservation: Insights from numerical tidal modelling in the Late Oligocene-Miocene South China Sea, Southeast Asia. Sedimentology 65, 2468–2505. https://doi.org/10.1111/sed.12474.

Dalrymple, R., Mackay, D., Ichaso, A., Choi, K., 2012. Processes, Morphodynamics, and Facies of Tide-Dominated Estuaries. In: Davis, R.A., Dalrymple, R.W. (Eds.) Principles of Tidal Sedimentology. Springer Science+Business Media B.V., Dordrecht.

Dalrymple, R., Zaitlin, B., Boyd, R., 1992. Estuarine facies models: Conceptual basis and stratigraphic implications. Journal of sedimentary petrology VOL. 62, No. 6, 1130–1146.

Dalrymple, R., Zaitlin, B.A., 1994. High-resolution sequence stratigraphy of a complex, incised valley succession, Cobequid Bay — Salmon River estuary, Bay of Fundy, Canada. Sedimentology 41, 1069–1091.

Dalrymple, R.W., Choi, K., 2007. Morphologic and facies trends through the fluvial–marine transition in tide-dominated depositional systems: A schematic framework for environmental and sequence-stratigraphic interpretation. Earth-Science Reviews 81, 135–174. https://doi.org/10.1016/j.earscirev.2006.10.002.

Davis, R., Dalrymple, R., 2012. Principles of Tidal Sedimentology. Springer Science+Business Media B.V., Dordrecht.

Dufois, F., Le Hir, P., 2015. Formulating Fine to Medium Sand Erosion for Suspended Sediment Transport Models. JMSE 3, 906–934. https://doi.org/10.3390/jmse3030906.

Ehrhold, A., Gregoire, G., 2015. SERABEQ-03 cruise,Thalia R/V.

Elmilady, H., Wegen, M., Roelvink, D., Spek, A., 2020. Morphodynamic Evolution of a Fringing Sandy Shoal: From Tidal Levees to Sea Level Rise. Journal of Geophysical Research: Earth Surface 125.

Fernane, A., 2014. Reconstitution des fluctuations holocènes en relation avec les changements climatiques et l'antropisation sur les côtes bretonnes à partir de bio-indicateurs fossiles (chironomidés, pollen et foraminifères benthiques), Brest, 248 pp.

Flemming, B., 2012. Siliciclastic Back-Barrier Tidal Flats. In: Davis, R.A., Dalrymple, R.W. (Eds.) Principles of Tidal Sedimentology. Springer Science+Business Media B.V., Dordrecht.

Franz, G., Delpey, M.T., Brito, D., Pinto, L., Leitão, P., Neves, R., 2017. Modelling of sediment transport and morphological evolution under the combined action of waves and currents. Ocean Science 13.

Frère, L., Paul-Pont, I., Rinnert, E., Petton, S., Jaffré, J., Bihannic, I., Soudant, P., Lambert, C., Huvet, A., 2017. Influence of environmental and anthropogenic factors on the composition, concentration and spatial distribution of microplastics: A case study of the Bay of Brest (Brittany, France). Environmental pollution (Barking, Essex : 1987) 225, 211–222. https://doi.org/10.1016/j.envpol.2017.03.023.

García-Artola, A., Stéphan, P., Cearreta, A., Kopp, R.E., Khan, N.S., Horton, B.P., 2018. Holocene sea-level database from the Atlantic coast of Europe. Quaternary Science Reviews 196, 177–192. https://doi.org/10.1016/j.quascirev.2018.07.031.

Goslin, J., van Vliet Lanoë, B., Spada, G., Bradley, S., Tarasov, L., Neill, S., Suanez, S., 2015. A new Holocene relative sea-level curve for western Brittany (France): Insights on isostatic dynamics along the Atlantic coasts of north-western Europe. Quaternary Science Reviews 129, 341–365. https://doi.org/10.1016/j.quascirev.2015.10.029.

Gregoire, G., 2016. Dynamique sédimentaire et évolution holocène d'un système macrotidal semi-fermé : l'exemple de la rade de Brest, Brest, 294 pp.

Gregoire, G., Ehrhold, A., Le Roy, P., Jouet, G., Garlan, T., 2016. Modern morpho-sedimentological patterns in a tide-dominated estuary system: the Bay of Brest (west Britanny, France). Journal of Maps 12, 1152–1159. https://doi.org/10.1080/17445647.2016.1139514.
Gregoire, G., Le Roy, P., Ehrhold, A., Jouet, G., Garlan, T., 2017. Control factors of Holocene sedimentary infilling in a semi-closed tidal estuarine-like system: the bay of Brest (France). Marine Geology 385, 84–100. https://doi.org/10.1016/j.margeo.2016.11.005.
Guo, L., van der Wegen, M., Roelvink, D., Wang, Z.B., He, Q., 2015. Long-term, process-based morphodynamic modeling of a fluvio-deltaic system, part I: The role of river discharge. Continental Shelf Research 109, 95–111. https://doi.org/10.1016/j.csr.2015.09.002.
Guo, L., Zhu, C., Xu, F., Xie, W., van der Wegen, M., Townend, I., Wang, Z.B., He, Q., 2022. Reclamation of Tidal Flats Within Tidal Basins Alters Centennial Morphodynamic Adaptation to Sea-Level Rise. JGR Earth Surface 127. https://doi.org/10.1029/2021JF006556.
Hallegouet, B., Lozac'h, G., Vigouroux, F., 1994. Formation de la Rade de Brest. Atlas permanent de la mer et du littoral n°1, 21.
Klouch, Z.K., Caradec, F., Plus, M., Hernández-Fariñas, T., Pineau-Guillou, L., Chapelle, A., Schmitt, S., Quéré, J., Guillou, L., Siano, R., 2016. Heterogeneous distribution in sediments and dispersal in waters of Alexandrium minutum in a semi-enclosed coastal ecosystem. Harmful algae 60, 81–91. https://doi.org/10.1016/j.hal.2016.11.001.
Koshkarova, V.L., Koshkarov, A.D., 2004. Regional signatures of changing landscape and climate of northern central Siberia in the Holocene. Geologiya I Geofizika 45(6), 717–729.
Lambert, C., 2017. Signature paléoenvironnementale des séquences holocènes en Rade de Brest : forçages climatiques et anthropiques, Brest, 248 pp.
Lanzoni, S., Seminara, G., 2002. Long-term evolution and morphodynamic equilibrium of tidal channels. J. Geophys. Res. 107. https://doi.org/10.1029/2000JC000468.
Lazure, P., Dumas, F., 2008. An external–internal mode coupling for a 3D hydrodynamical model for applications at regional scale (MARS). Advances in Water Resources 31, 233–250. https://doi.org/10.1016/j.advwatres.2007.06.010.
Le Hir, P., Cayocca, F., Waeles, B., 2011. Dynamics of sand and mud mixtures: A multiprocess-based modelling strategy. Continental Shelf Research 31, 135-149. https://doi.org/10.1016/j.csr.2010.12.009.
Le Roy, R., Simon, B., 2003. Réalisation et validation d'un modèle de marée en Manche et dans le Golfe de Gascogne(application à la réalisation d'un nouveau programme de réduction des sondages bathymétrique. Rapport technique Rapport n002/03.
Le Tu, X., Thanh, V.Q., Reyns, J., Van, S.P., Anh, D.T., Dang, T.D., Roelvink, D., 2019. Sediment transport and morphodynamical modeling on the estuaries and coastal zone of the Vietnamese Mekong Delta. Continental Shelf Research 186, 64–76. https://doi.org/10.1016/j.csr.2019.07.015.
Lee, B.-R., Yoo, D.-G., Lee, G.-S., 2022. High-resolution sequence stratigraphy and evolution of the Jeju Strait shelf, Korea, since the Last Glacial Maximum. Marine and Petroleum Geology 135, 105389. https://doi.org/10.1016/j.marpetgeo.2021.105389.
Lemoine, J.P., Le Hir, P., 2021. Maintenance dredging in a macrotidal estuary: Modelling and assessment of its variability with hydro-meteorological forcing. Estuarine, Coastal and Shelf Science 258, 107366. https://doi.org/10.1016/j.ecss.2021.107366.
Mengual, B., Hir, P., Cayocca, F., Garlan, T., 2017. Modelling Fine Sediment Dynamics: Towards a Common Erosion Law for Fine Sand, Mud and Mixtures. Water 9, 564. https://doi.org/10.3390/w9080564.
Mitchell, A.J., Uličný, D., Hampson, G.J., Allison, P.A., Gorman, G.J., Piggott, M.D., Wells, M.R., Pain, C.C., 2010. Modelling tidal current-induced bed shear stress and palaeocirculation in an

epicontinental seaway: the Bohemian Cretaceous Basin, Central Europe. Sedimentology 57, 359–388. https://doi.org/10.1111/j.1365-3091.2009.01082.x.
Monbet, Y., Bassoullet, P., 1989. Bilan des connaissances océanographiques en rade de Brest. Rapport CEA/IPSN, code DERO/EL 89-23.
Nielsen, P., 1992. Coastal bottom boundary layers and sediment transport. Advanced series on Ocean Engineering. World Scientific.
Olariu, C., Steel, R.J., Dalrymple, R.W., Gingras, M.K., 2012. Tidal dunes versus tidal bars: The sedimentological and architectural characteristics of compound dunes in a tidal seaway, the lower Baronia Sandstone (Lower Eocene), Ager Basin, Spain. Sedimentary Geology 279, 134–155. https://doi.org/10.1016/j.sedgeo.2012.07.018.
Olivier, M.G., Leroux, E., Rabineau, M., Le Hir, P., Granjeon, D., Chataigner, T., Beudin, A., Muller, H., 2021. Numerical modelling of a Macrotidal Bay over the last 9,000 years: An interdisciplinary methodology to understand the influence of sea-level variations on tidal currents in the Bay of Brest. Continental Shelf Research 231, 104595. https://doi.org/10.1016/j.csr.2021.104595.
Penaud, A., Ganne, A., Eynaud, F., Lambert, C., Coste, P.O., Herlédan, M., Vidal, M., Goslin, J., Stéphan, P., Charria, G., Pailler, Y., Durand, M., Zumaque, J., Mojtahid, M., 2020. Oceanic versus continental influences over the last 7 kyrs from a mid-shelf record in the northern Bay of Biscay (NE Atlantic). Quaternary Science Reviews 229, 106135. https://doi.org/10.1016/j.quascirev.2019.106135.
Petton, S., Pouvreau, S., Dumas, F., 2020. Intensive use of Lagrangian trajectories to quantify coastal area dispersion. Ocean Dynamics 70, 541–559. https://doi.org/10.1007/s10236-019-01343-6.
Price, W.A., Kendrick, M.P., 1963. Field and model investigation into the reasons for siltation in the Mersey estuary. Proceedings of the Institution of Civil Engineers 24 (4), 473–518.
Rees, J.G., Ridgway, J., Ellis, S., Knox, R.W.O., Newsham, R., Parkes, A., 2000. Holocene sediment storage in the Humber Estuary. in : Holocene Land-ocean interaction and environmental change around the North Sea, Shennan, I. and Andrews, J. E. (eds). Geological Society, London, Special Publications 166, 119–143.
Reynaud, J.-Y., Dalrymple, R.W., 2012. Shallow-Marine Tidal Deposits. In: Davis, R.A., Dalrymple, R.W. (Eds.) Principles of Tidal Sedimentology, vol. 13. Springer Science+Business Media B.V., Dordrecht, pp. 335–369.
Reynaud, J.-Y., Dalrymple, R.W., Vennin, E., Parize, O., Besson, D., Rubino, J.-L., 2006. Topographic Controls on Production and Deposition of Tidal Cool-Water Carbonates, Uzes Basin, SE France. Journal of Sedimentary Research 76, 117–130. https://doi.org/10.2110/jsr.2006.07.
Reynaud, J.-Y., James, N.P., 2012. The Miocene Sommières basin, SE France: Bioclastic carbonates in a tide-dominated depositional system. Sedimentary Geology 282, 360–373. https://doi.org/10.1016/j.sedgeo.2012.10.006.
Roelvink, J.A., 2006. Coastal morphodynamic evolution techniques. Coastal Engineering 53, 277–287.
Seppä, H., Birks, H., 2001. July mean temperature and annual precipitation trends during the Holocene in the ennoscandian tree-line area: pollen-based climate reconstructions. The Holocene 11,5, 527–539.
Shanmugam, G., Shrivastava, S.K., Das, B., 2009. Sandy Debrites and Tidalites of Pliocene Reservoir Sands in Upper-Slope Canyon Environments, Offshore Krishna-Godavari Basin (India): Implications. Journal of Sedimentary Research 79, 736–756. https://doi.org/10.2110/jsr.2009.076.
Soulsby, R., 1997. Dynamics of marine sands. Thomas Telford Publications, 249p.
Stéphan, P., Fichaut, B., Suanez, S., 2012. Les sillons de la rade de Brest et les marais maritimes associés. FRAC GPN, 137 pp.

Tessier, B., 2012. Stratigraphy of Tide-Dominated Estuaries. In: Davis, R.A., Dalrymple, R.W. (Eds.) Principles of Tidal Sedimentology. Springer Science+Business Media B.V., Dordrecht.

Tessier, B., Billeaud, I., Sorrel, P., Delsinne, N., Lesueur, P., 2012. Infilling stratigraphy of macrotidal tide-dominated estuaries. Controlling mechanisms: Sea-level fluctuations, bedrock morphology, sediment supply and climate changes (The examples of the Seine estuary and the Mont-Saint-Michel Bay, English Channel, NW France). Sedimentary Geology 279, 62–73. https://doi.org/10.1016/j.sedgeo.2011.02.003.

Tosic, M., Martins, F., Lonin, S., Izquierdo, A., Restrepo, J, D., 2019. Hydrodynamic modelling of a polluted tropical bay_ Assessment of anthropogenic impacts on freshwater runoff and estuarine water renewal. Journal of Environmental Management 236, 695–714.

Townend, I., Wang, Z., Rees, J., 2007. Millennial to annual volume changes in the Humber Estuary. Proc. R. Soc. A. 463, 837–854. https://doi.org/10.1098/rspa.2006.1798.

Townend, I., Zhou, Z., Guo, L., Coco, G., 2021. A morphological investigation of marine transgression in estuaries. Earth Surf. Process. Landforms 46, 626–641. https://doi.org/10.1002/esp.5050.

Uehara, K., Scourse, J.D., Horsburgh, K.J., Lambeck, K., Purcell, A.P., 2006. Tidal evolution of the northwest European shelf seas from the Last Glacial Maximum to the present. J. Geophys. Res. 111. https://doi.org/10.1029/2006JC003531.

van Rijn, L., 1994. Sediment Transport, Part I: Bed Load Transport. J. Hydraul. Eng. 110(10), 1431–1456.

Wang, P., 2012. Principles of Sediment Transport Applicable in Tidal Environments. In: Davis, R.A., Dalrymple, R.W. (Eds.) Principles of Tidal Sedimentology. Springer Science+Business Media B.V., Dordrecht.

Ward, S.L., Neill, S.P., Scourse, J.D., Bradley, S.L., Uehara, K., 2016. Sensitivity of palaeotidal models of the northwest European shelf seas to glacial isostatic adjustment since the Last Glacial Maximum. Quaternary Science Reviews 151, 198–211. https://doi.org/10.1016/j.quascirev.2016.08.034.

Wells, M.R., Allison, P.A., Piggott, M.D., Gorman, G.J., Hampson, G.J., Pain, C.C., Fang, F., 2007a. Numerical Modeling of Tides in the Late Pennsylvanian Midcontinent Seaway of North America with Implications for Hydrography and Sedimentation. Journal of Sedimentary Research 77, 843–865. https://doi.org/10.2110/jsr.2007.075.

Wells, M.R., Allison, P.A., Piggott, M.D., Hampson, G.J., Pain, C.C., Gorman, G.J., 2010. Tidal Modeling of an Ancient Tide-Dominated Seaway, Part 1: Model Validation and Application to Global Early Cretaceous (Aptian) Tides. Journal of Sedimentary Research 80, 393–410. https://doi.org/10.2110/jsr.2010.044.

Wells, M.R., Allison, P.A., Piggott, M.D., Pain, C.C., Hampson, G.J., Dodman, A., 2007b. Investigating tides in the Early Pennsylvanian Seaway of NW Eurasia using the Imperial College Ocean Model. Geological Association of Canada,St. John's, Newfoundland Special paper 48, 363–387.

Zhou, Z., Coco, G., Townend, I., Olabarrieta, M., van der Wegen, M., Gong, Z., D'Alpaos, A., Gao, S., Jaffe, B.E., Gelfenbaum, G., He, Q., Wang, Y., Lanzoni, S., Wang, Z., Winterwerp, H., Zhang, C., 2017. Is "Morphodynamic Equilibrium" an oxymoron? Earth-Science Reviews 165, 257–267. https://doi.org/10.1016/j.earscirev.2016.12.002.

Zuchuat, V., Steel, E., Mulligan, R.P., Collins, D.S., Green, J.M., 2022. Tidal dynamics in palaeo-seas in response to changes in physiography, tidal forcing and bed shear stress. Sedimentology. https://doi.org/10.1111/sed.12975.

Numerical Modelling of Tidal Sediment Dynamics in the Bay of Brest over the Holocene: How the Use of a Process-Based Model over Paleoenvironmental Reconstitutions can Help Understand Long-term Tidal Deposits?

Matthieu Guillaume Olivier[a,b,c*], Estelle Leroux[d], Didier Granjeon[c], Pierre Le Hir[b], Marina Rabineau[d], Pascal Le Roy[a], Laure Simplet[e], Axel Ehrhold[a], Héloïse Muller[b]

a IFREMER/IUEM – ASTRE laboratory – UMR Geo-Ocean – Pointe du Diable, 29280 Plouzané, France

b IFREMER – DYNECO/DHYSED laboratory – Pointe du Diable, 29280, Plouzané, France

c IFP Énergies nouvelles – 1 et 4, avenue de Bois-Préau, 92500, Rueil-Malmaison, France

d IFREMER/IUEM – GIPS laboratory – UMR Geo-Ocean – Pointe du Diable, 29280 Plouzané, France

e IFREMER/IUEM – ODYSC laboratory – UMR Geo-Ocean – Pointe du Diable, 29280 Plouzané, France

Supplementary materials

Supplementary materials of this article contain 13 figures. Figure 1 aims to give an over view of bottom current velocities evolution over the scenarios and displays the impact of rivers water discharges modifications. Figure 2 also displays the impact of rivers modifications, but on bathymetric evolution of scenario 1. Figure 3 shows the evolution of suspended sediment volume over spring tides and highlights the tidal asymmetry in the Bay of Brest. Figures 4 to 9 are the core logs (corelated with seismic profiles) used for the validation of grain size classes distribution. Finally, Figures 10 to 13, and the text included with those figures, detail the comparison between grain size classes erosion and deposition simulated and sediment records.

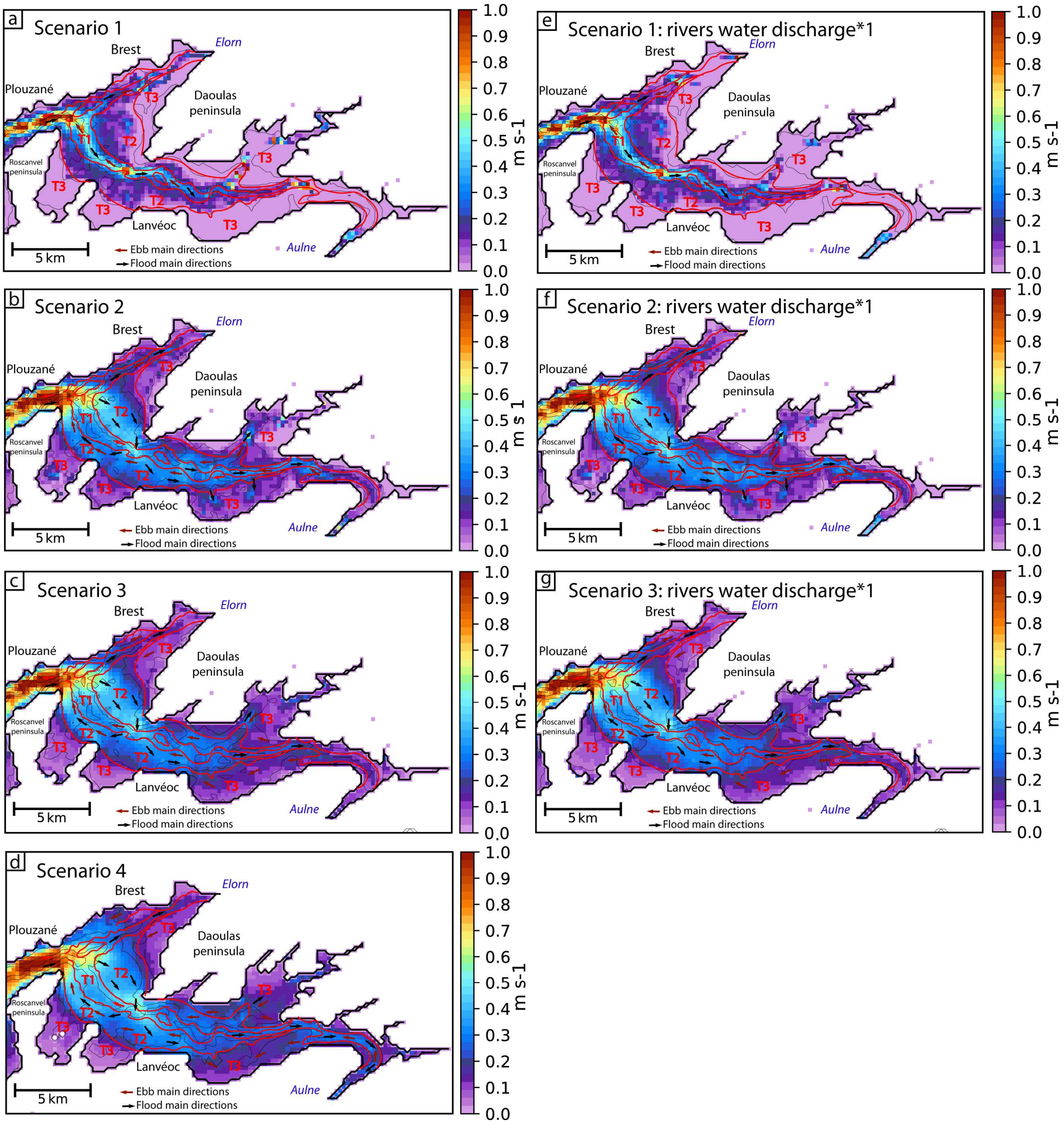

Fig. 1: Bottom current percentile 90 over one year for a: scenario 1, b: scenario 2, c: scenario 3, d: scenario 4, e: scenario 1 with a water river discharge equal to scenario 4, f: scenario 2 with a water river discharge equal to scenario 4, g: scenario 3 with a water river discharge equal to scenario 4.

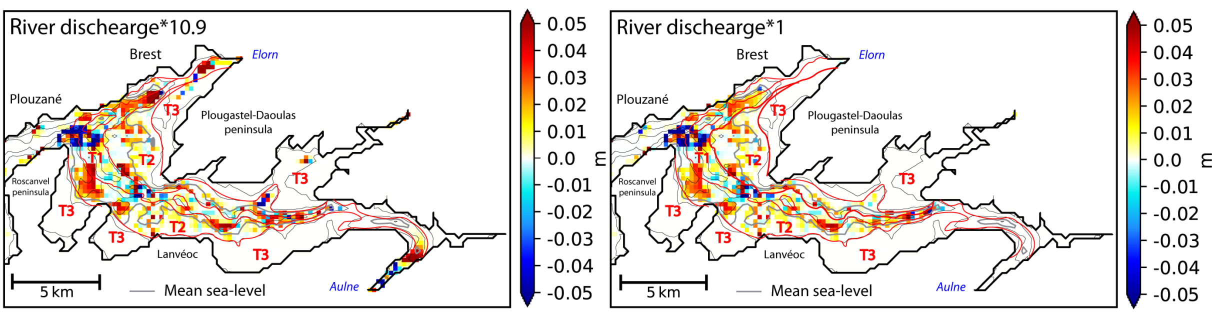

Fig. 2: On the left, bathymetric evolution after 1 year for scenario 1 (9 ka BP) and on the right bathymetric evolution after 1 year for scenario 1, with a river water discharge equal to scenario 4. Red lines are morphological domain limits (T1, T2 T3) and the black line is the present-day coastline. Grey lines represent the mean sea level (-26 m).

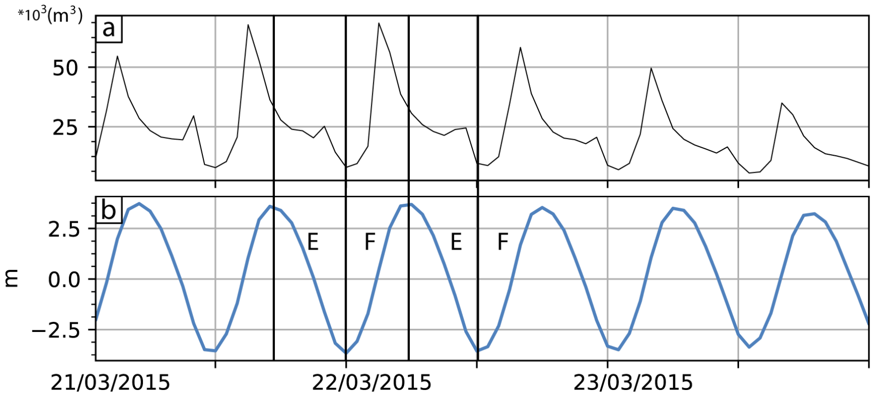

Fig. 3: (a) Evolution of suspended matter volume over the Bay through time over spring tides for the present-day configuration (scenario 4, computational limits on Fig. 3 of the manuscript). (b) Evolution of sea surface variations at the entrance of the Bay (central area). F: Flood tide; E: Ebb tide.

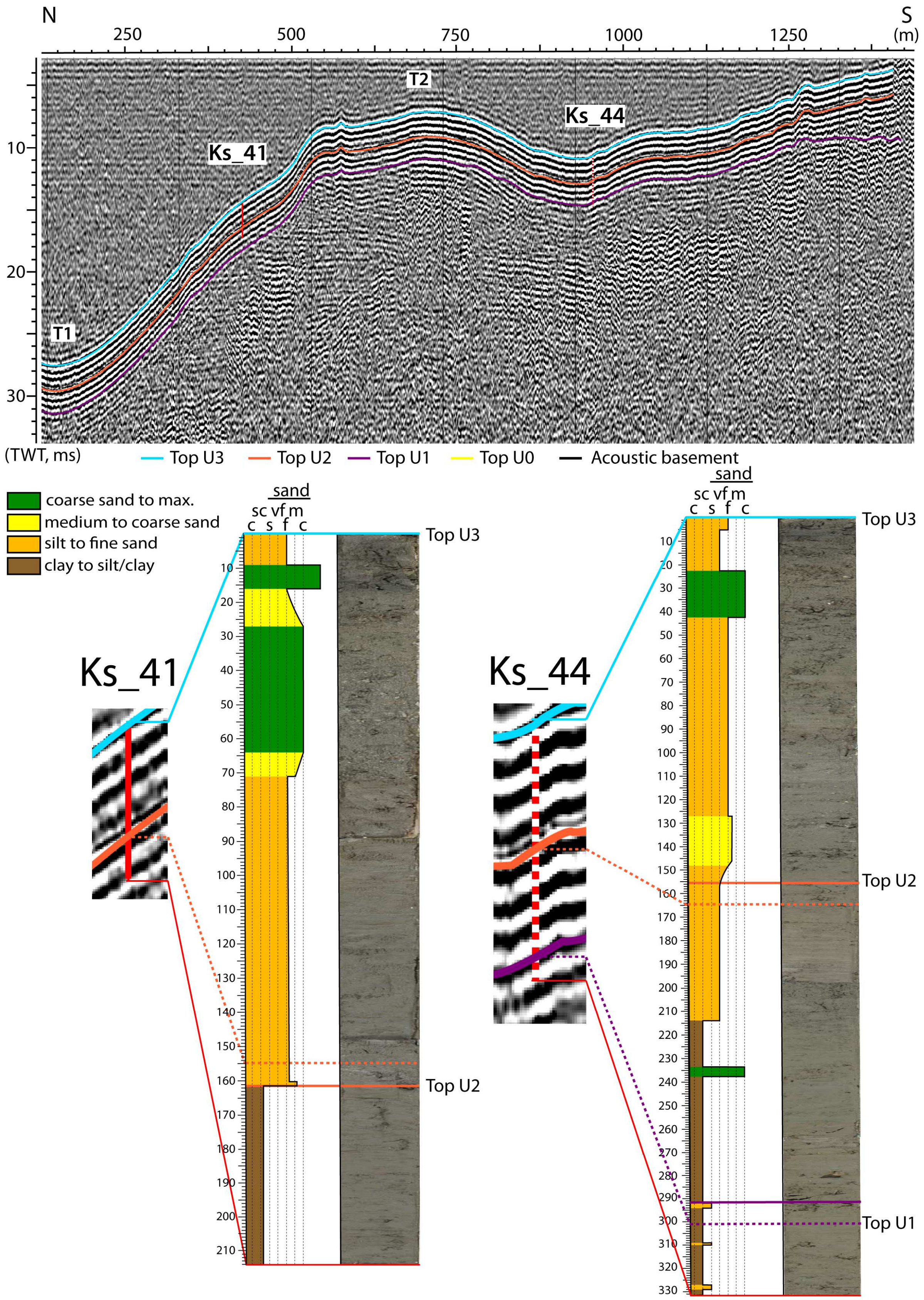

Fig. 4: (top) Interpreted seismic profile (location on Fig. 3b of the manuscript). (bottom) Photographs and lithologic logs for cores Ks_41 and Ks_44. Dashed purple and orange lines are markers from seismic interpretation and full purple and orange lines represent the interpreted top of U1 and U2 (made to compensate the difference of resolution between cores and seismic profile).

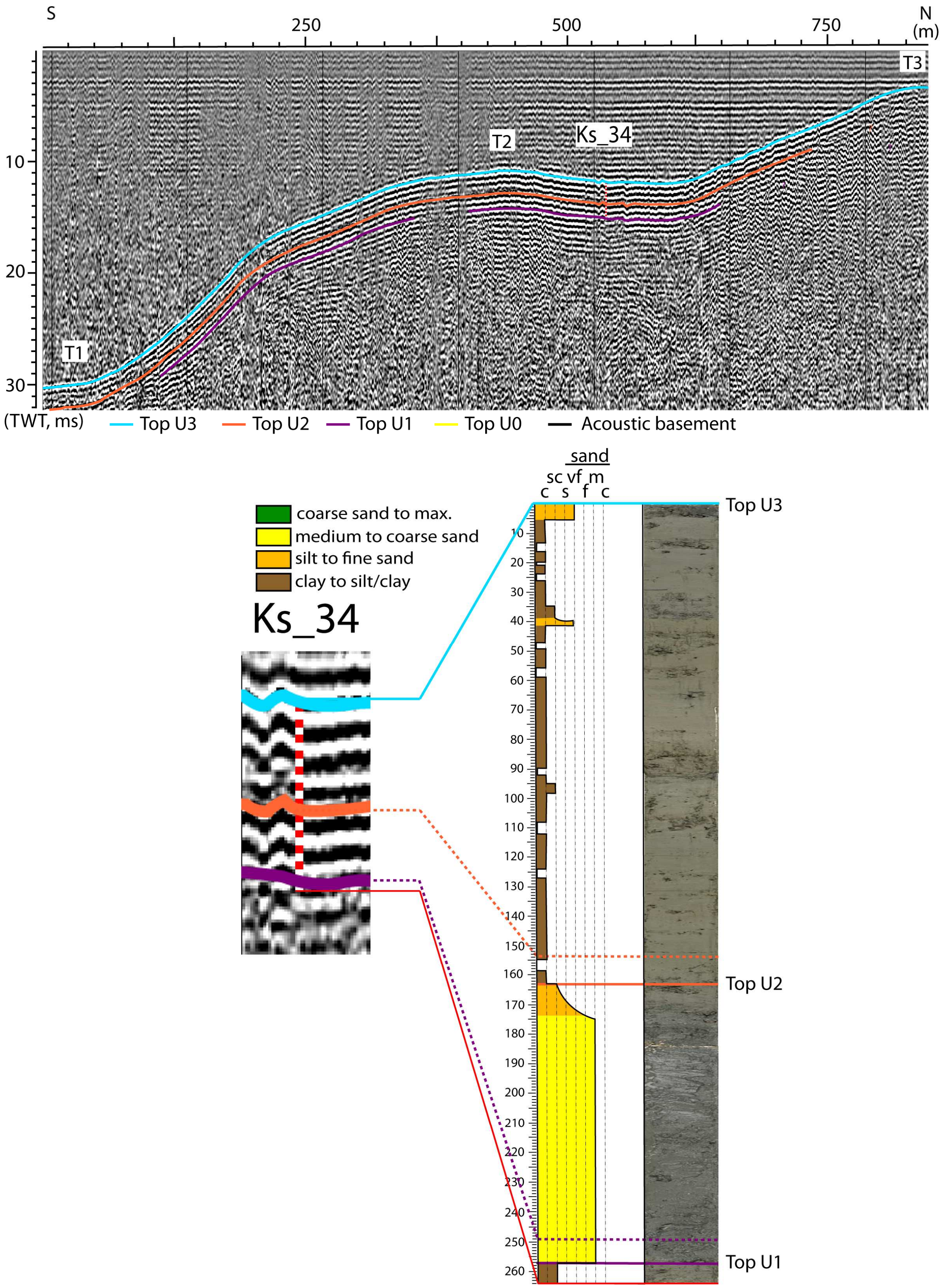

Fig. 5: (top) Interpreted seismic profile (location on Fig. 3b of the manuscript). (bottom) Photograph and lithologic logs for cores Ks_41 and Ks_44. Dashed purple and orange lines are markers from seismic interpretation and full purple and orange lines represent the interpreted top of U1 and U2 (made to compensate the difference of resolution between cores and seismic profile).

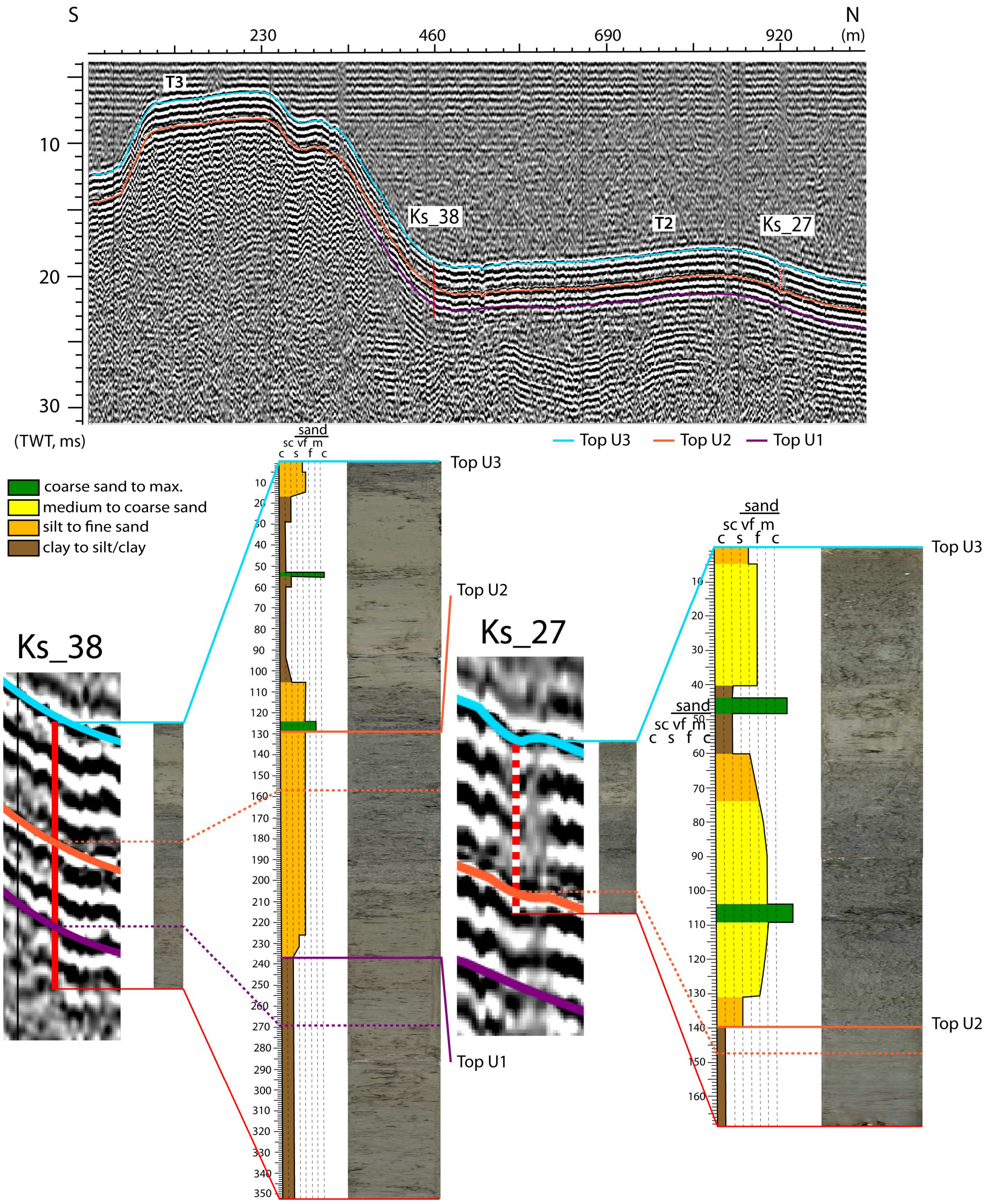

Fig. 6: (top) Interpreted seismic profile (location on Fig. 3b of the manuscript). (bottom) Photographs and lithologic log for cores Ks_38 and Ks_27. Dashed purple and orange lines are markers from seismic interpretation and full purple and orange lines represent the interpreted top of U1 and U2 (made to compensate the difference of resolution between cores and seismic profile).

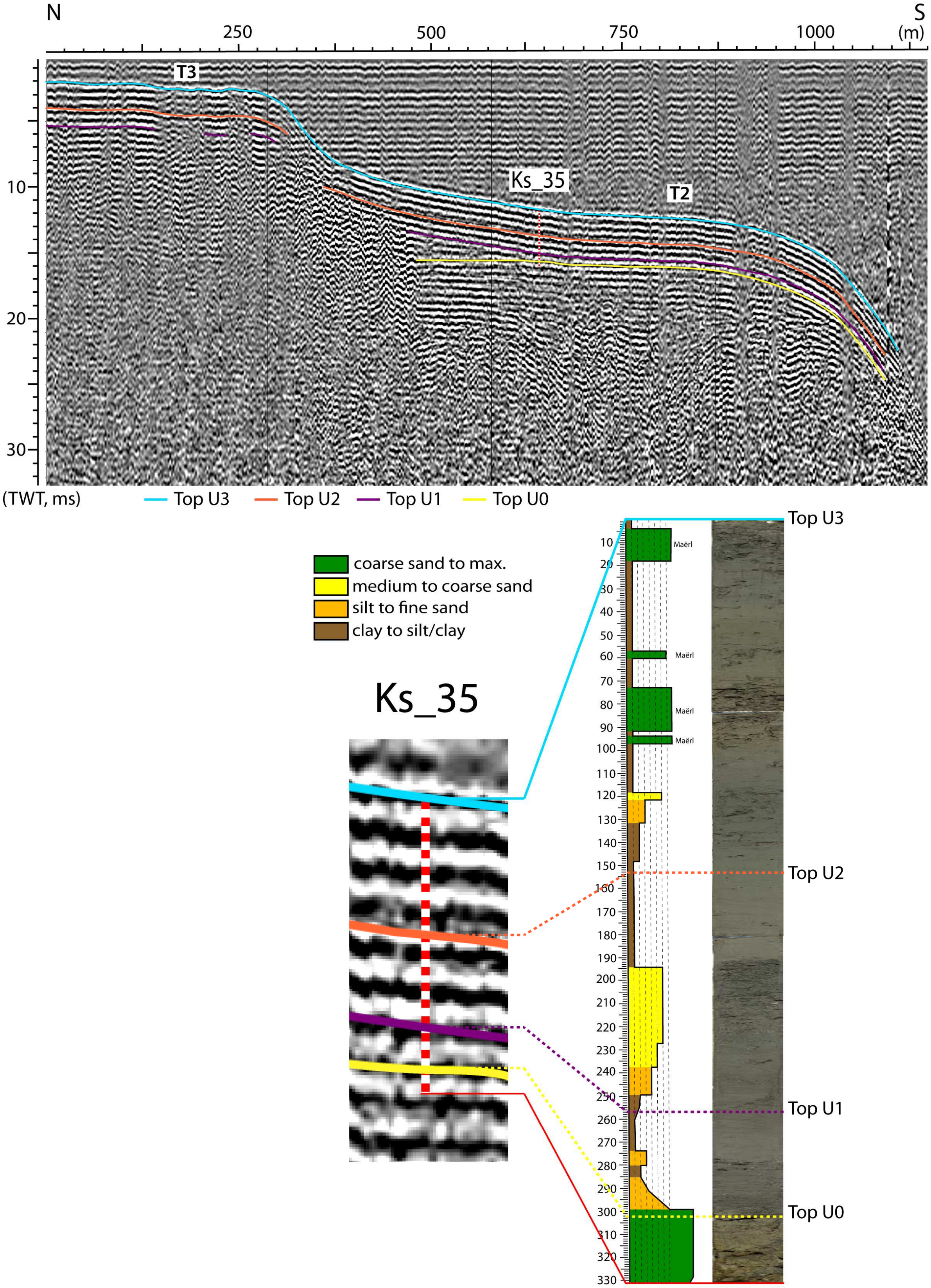

Fig. 7: (top) Interpreted seismic profile (location on Fig. 3b of the manuscript). (bottom) Photograph and lithologic log for core Ks_35. Maërl: only bioconstructions of Maërls.

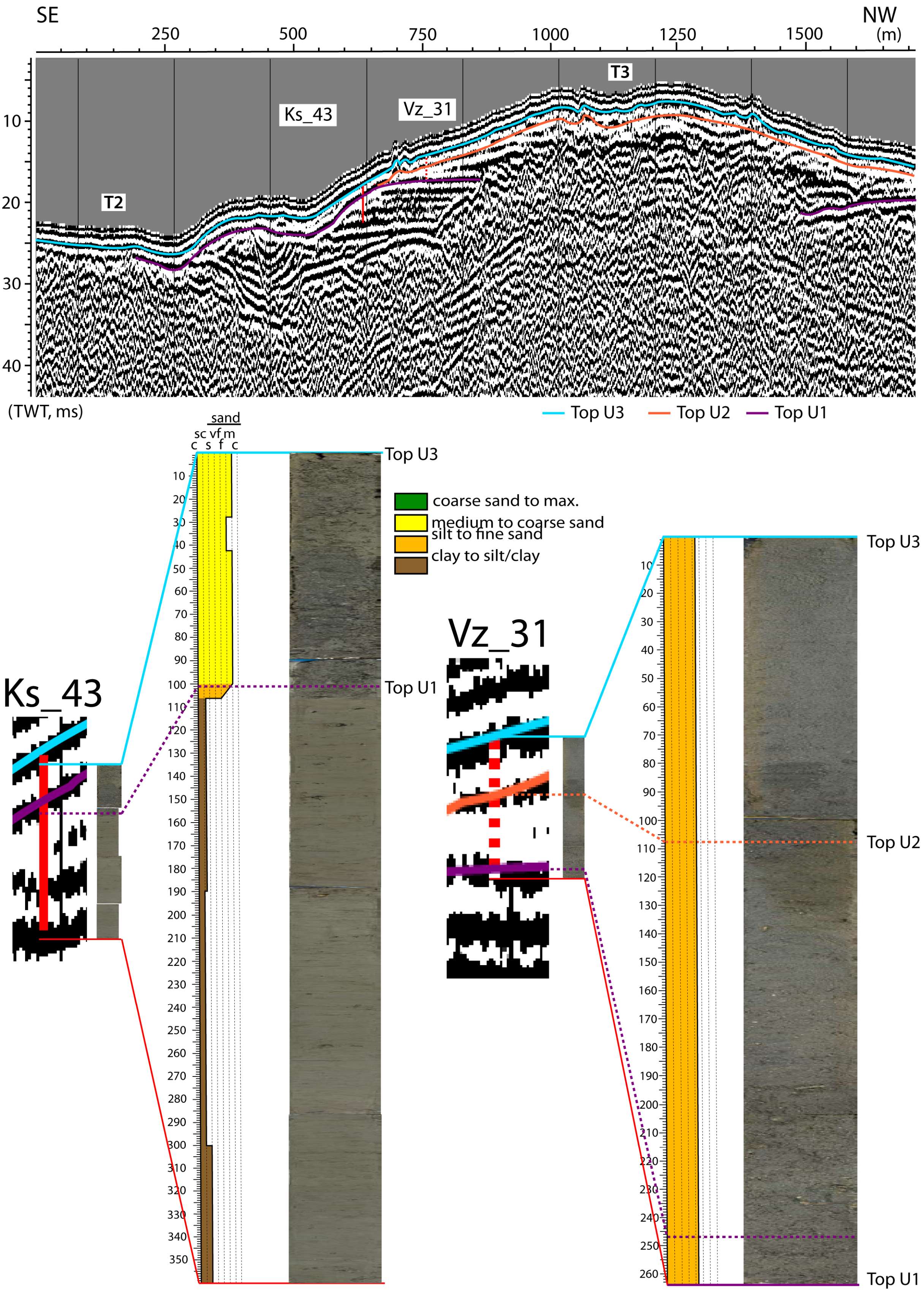

Fig. 8: (top) Interpreted seismic profile (location on Fig. 3b of the manuscript). (bottom) Photographs and lithologic log for cores Ks_43 and Vz_31.

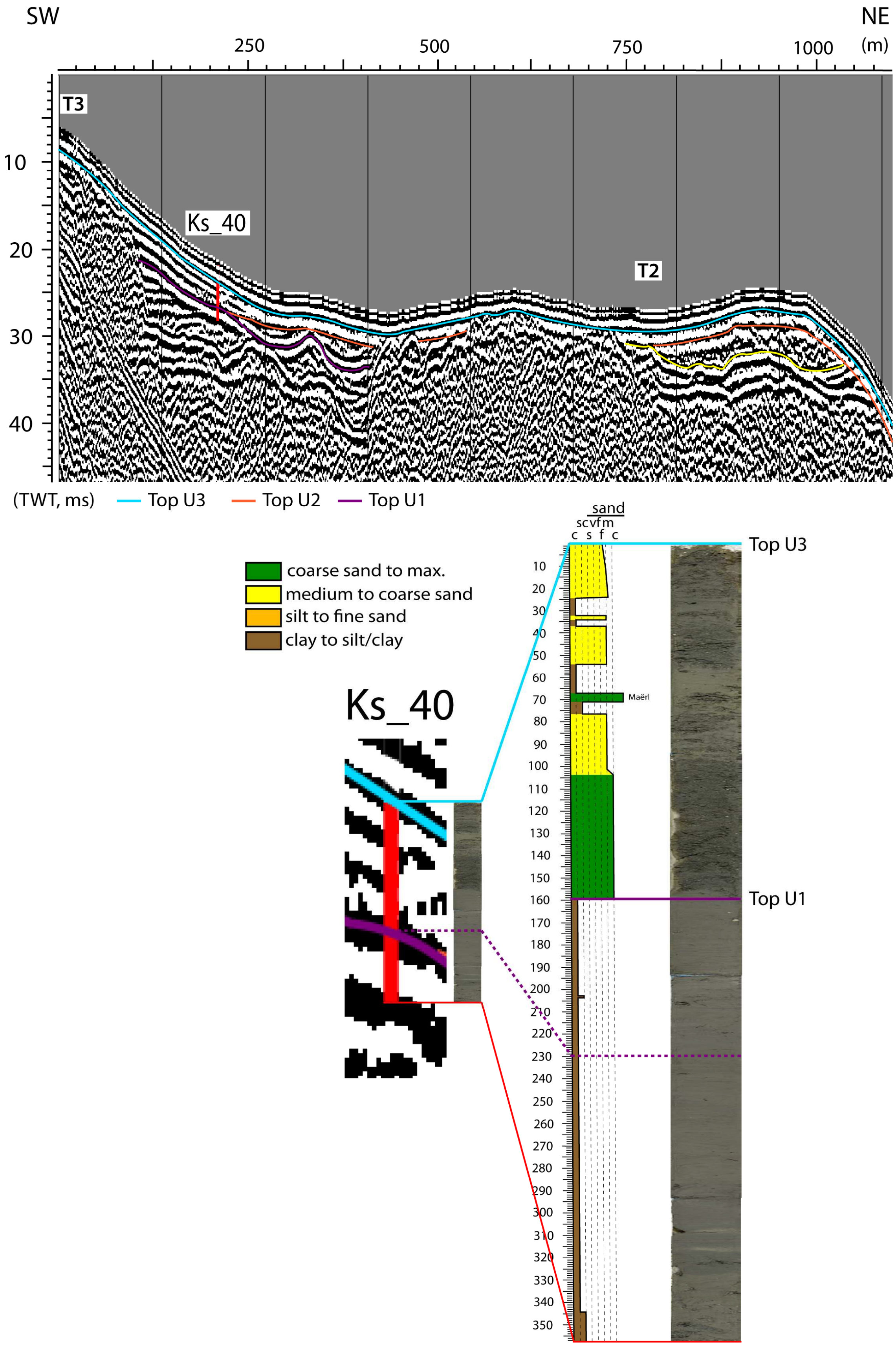

Fig. 9: (top) Interpreted seismic profile (location on Fig. 3b of the manuscript). (bottom) Photograph and lithologic log for core Ks_40. Dashed purple line is marker from seismic interpretation and full purple line represents the interpreted top of U1 (made to compensate the difference of resolution between cores and seismic profile). Maërl: only bioconstructions of Maërls.

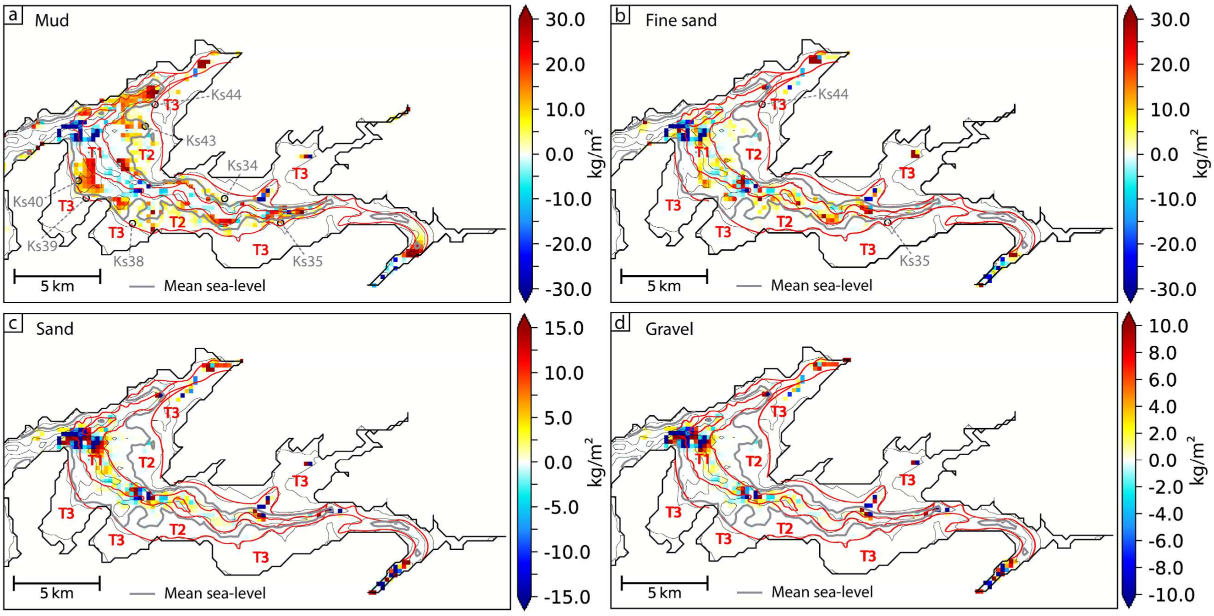

Fig. 10: Grain-size class erosion and deposition after 1 year for scenario 1 (9 – 7.5 ka BP): a mud, b fine sand, c sand, d gravel. Black circles show where the corresponding grain-size classes were recorded by cores. Core names are available in grey and red lines are morphological domain limits.

At each core location or very close (one cell of the computation grid) where muds are observed, mud deposits are simulated (Fig. 10a, Tab. 6 of the manuscript, Ks_34, Ks_35, Ks_38, Ks_39, Ks_40, Ks_43 and Ks_44). All non-cohesive sediment classes (fine sand, sand and gravel) are mostly present over T1, only some fine sands are present in secondary channels and reach some areas of T2 (Figs. 10b, 10c, 10d). Unfortunately, cores are available mostly at the interface between T2 and T3. However, two cores present fine sand accumulations (Ks_35 and Ks_44) and no fine sand deposit is simulated at the beginning of U1 at these locations (Fig. 10b).

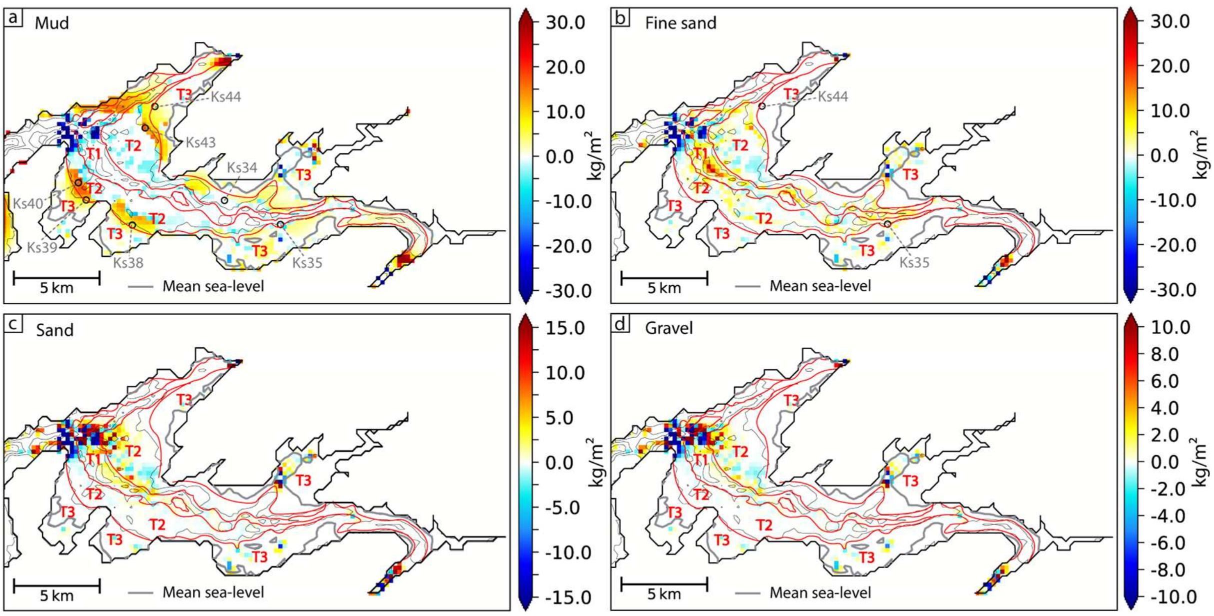

Fig. 11: Grain-size class erosion and deposition after 1 year for scenario 2 (7.5 – 7 ka BP): a mud, b fine sand, c sand, d gravel. Black circles show where the corresponding grain-size classes were recorded by cores. Core names are available in grey and red lines are morphological domain limits.

All the cores presenting mud records (Fig. 11a, Ks_38, Ks_39, Ks_40, Ks_43 and Ks_44) are located where mud deposits are simulated, except for Ks_34 and Ks_35. At Ks_34 and Ks_35 locations, the balance between erosion and deposition is close to 0 (Fig. 11a), but mud deposits are simulated during scenario 1 (Fig. 10a). If no erosion is simulated during scenario 2 (end of U1), deposits from the beginning of U1 (scenario 1) should be preserved and are indeed observed inside cores (Ks_34 and Ks_35). Cores on slopes between T2 and T3, do corroborate this simulation result as they display only mud and fine sand. Fine sand deposit is observed in Ks_44 and is simulated close to the ks_44 location. In the upper area, slight movements of sand and gravel are simulated over T1 and secondary channels, but over these areas, only fine sands are deposited over T1 and secondary channels in smaller quantity than in the centre (around 5 kg/m², Figs. 11b, 11c, 11d). Fine sands are observed inside core Ks35, which is located in a secondary channel in the upper area (Fig. 11b). Deposits simulated in T1 are impossible to confirm by field data as no cores are available in this morphological domain. However, the seismic facies were interpreted as coarse sediments (Gregoire, 2016) and would therefore corroborate the simulation results.

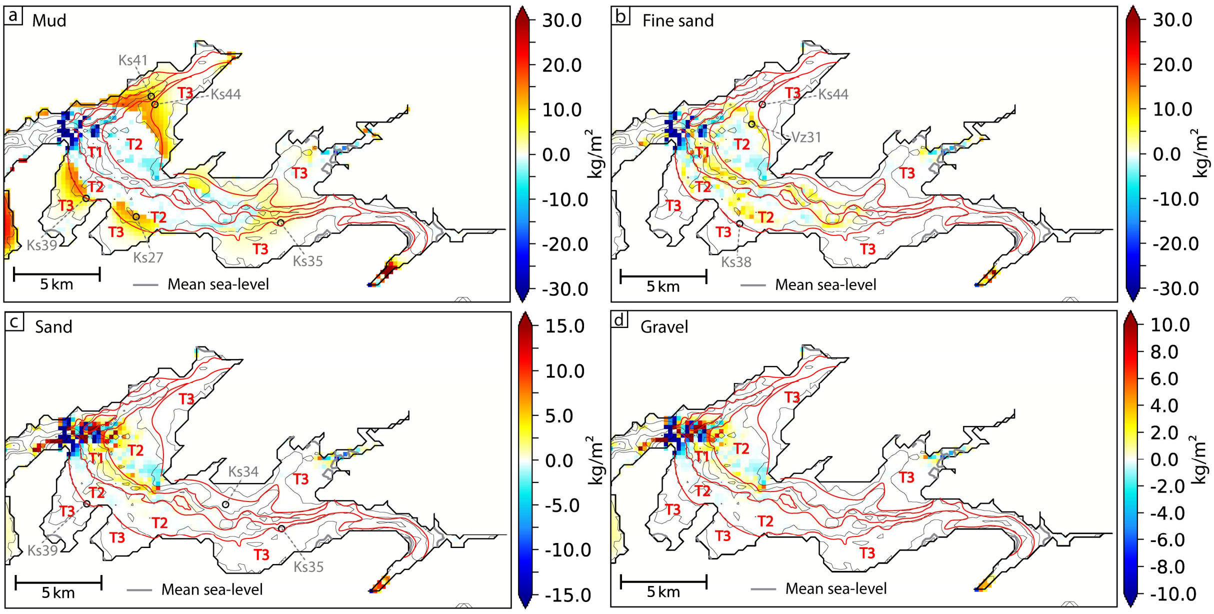

Fig. 12: Grain-size class erosion and deposition after 1 year for scenario 3 (6.8 – 3 ka BP): a mud, b fine sand, c sand, d gravel. Black circles show where the corresponding grain-size classes were recorded by cores. Core names are available in grey and red lines are morphological domain limits.

Mud deposits are recorded in Ks_35, but the two cores available in the upper part also display sands (Ks_34 and Ks_35, Fig. 12c). Mud deposits are also observed in cores Ks_27, Ks_39, Ks_41 and Ks_44 in the centre (Fig. 12a), where mud deposits are simulated. Observations of cores Ks_38, Ks_39, Ks_44 and Vz_31 show fine sands and sand on slopes between T2 and T3 and fine-sand deposits are simulated close to the three core locations (Fig. 12b). Ks_39 reveals the presence of some sand on the slope between T2 and T3, but very few deposits of sand are simulated close to core Ks_39 (Fig. 12c, less than 1 kg/m²).

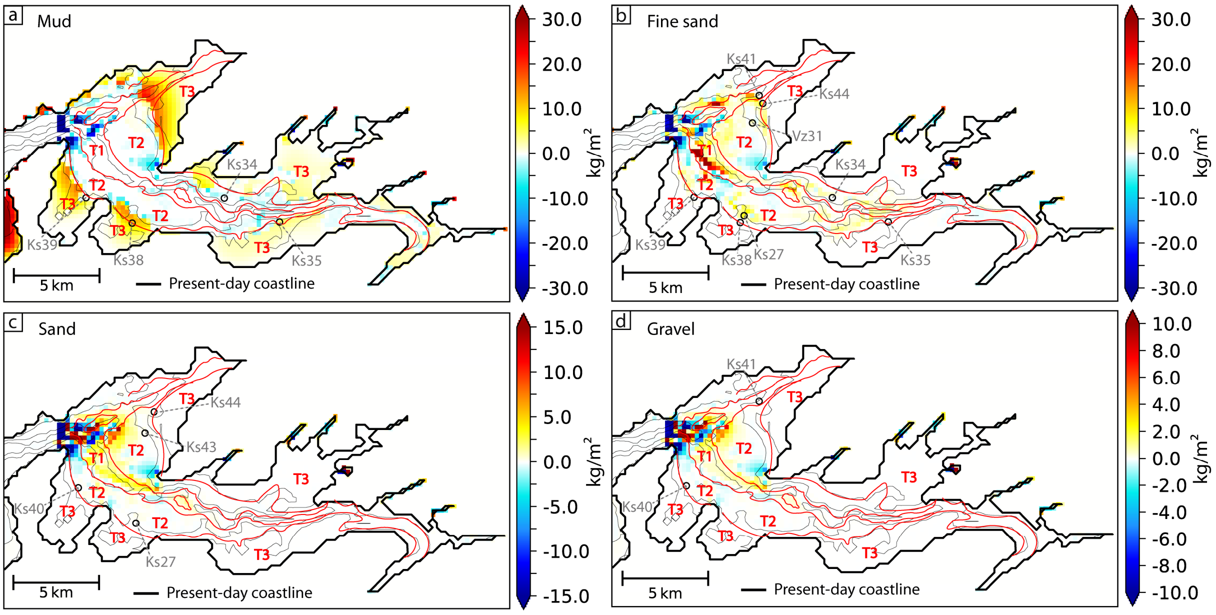

Fig. 13: Grain-size class erosion and deposition *after 1 year for scenario 4 (present-day): a mud, b fine sand, c sand, d gravel. Black circles show where the corresponding grain-size classes were recorded by cores. Core names are available in grey and red lines are morphological domain limits.*

Muds are observed only in Ks_35, Ks_38, Ks_39 (T3) and Ks_34 (T2), but at the Ks_34 location, no mud deposit is simulated. Fine-sand deposits are simulated close to cores that also show fine-sand (Fig. 13b, Ks_27, Ks_34, Ks_35, Ks_38, Ks_39, Ks_41, Ks_44, Vz_31). Sands simulated and observed in cores (Ks_27, Ks_40, Ks_43, Ks_44) also make a good match, even if small quantities are simulated at these core locations (around 1 kg/m², Fig. 13c). Also note that two cores (Ks_40 and Ks_41) show gravel deposit that is not simulated, close to T1 in the north of the central part and on slopes between T2 and T3 in the south. The presence of gravel deposits in two cores is unexplained by the tidal process.

Global trends of erosion/deposition patterns between simulation and data fit well. However, there are some mismatches between the simulations and the geological data: the presence of sands (observed in Ks_34 and Ks_35) in the upper zone during scenario 3 and gravels (observed in Ks_40 and Ks_41) in the centre during scenario 4 remains unexplained by simulations (Figs. 12 and 13 respectively). Simulated tidal currents are not able to transport sands and gravels at these core locations, and therefore it is difficult to link such coarse deposits to tide-induced hydrodynamics (Olivier et al., 2021, Figs. 12 and 13). They are potentially due to non-simulated extreme events, such as storm winds. Such energetic events could be able to transport coarse sediments into the Bay, without later remobilisation by weaker tide-induced currents. They should therefore be recorded in the cores (unless they reach T2 in the centre, which is the only morphological domain where tidal currents can transport sands and gravels during scenarios 2, 3 and 4). Ehrhold et al. (2021) observed storm patterns within some sedimentary facies of units U2 and U3 that may correspond to the coarsest deposits we also observed. The presence of these coarse sediments underlines the importance of climatic variations on sediment supply in estuaries.

References

Ehrhold, A., Jouet, G., Le Roy, P., Jorry, S.J., Grall, J., Reixach, T., Lambert, C., Gregoire, G., Goslin, J., Roubi, A., Penaud, A., Vidal, M., Siano, R., 2021. Fossil maerl beds as coastal indicators of late Holocene palaeo-environmental evolution in the Bay of Brest (Western France).

Gregoire, G., 2016. Dynamique sédimentaire et évolution holocène d'un système macrotidal semi-fermé. l'exemple de la rade de Brest, Brest, p. 294.